12-2005

Determination of Stiffness Matrix of Tapered Roller Bearings for Vibration Models

Jeeva Kumar

DETERMINATION OF STIFFNESS MATRIX OF TAPERED ROLLER BEARINGS FOR VIBRATION MODELS

by

Jeeva Kumar

A Thesis
Submitted to the
Faculty of The Graduate College
in partial fulfillment of the
requirements for the
Degree of Master of Science in Engineering (Mechanical)
Department of Mechanical and Aeronautical Engineering

Western Michigan University
Kalamazoo, Michigan
December 2005

ACKNOWLEDGMENTS

I would like to start by expressing my acknowledgement to my advisor, Dr. Richard. B. Hathaway for his continuous encouragement and thoughtful guidance throughout this thesis and also throughout my graduate studies. I would also like to thank Dr. Caner Demirdogen, Dana Corporation, for his excellent guidance and appreciation throughout the stages of this research. I also wish to thank Paul Pollock, Chief Engineer, Dana Corporation, for funding this research. Thanks are also due to Jim Ridge, Dana Corporation, for his time during the initial stages of the research. Also, I wish to thank Glenn Hall and Peter Thannhauser, staff, Western Michigan University, for their time in helping complete the tests.

I would also like to thank my mother and my wife Latha, for their continuous encouragement during my studies in the United States.

Jeeva Kumar

DETERMINATION OF STIFFNESS MATRIX OF TAPERED ROLLER BEARINGS FOR VIBRATION MODELS

Jeeva Kumar, M.S.E.

Western Michigan University, 2005

The stiffness matrix of tapered roller bearings under radial and axial load conditions was evaluated using an analytical model and an experimental approach. An experimental test system was designed and manufactured to determine the radial stiffness of the bearing under combined axial and radial load conditions. A second fixture was designed to measure the stiffness of the bearing under pure axial load conditions. The stiffness coefficients determined have been compared with those obtained from the analytical model, OEM (Original Equipment Manufacturer) data and ABAQUS model (finite element analysis software).

TABLE OF CONTENTS

Table of Contents—Continued

Table of Contents—Continued

LIST OF TABLES

LIST OF FIGURES

List of Figures—Continued

NOMENCLATURE

$(\delta)_{rj}$	effective j^{th} rolling element displacement in the radial direction
$(\delta)_{zj}$	effective j^{th} rolling element displacement in the axial direction
δ_{Rj}	resultant elastic deformation of the j^{th} rolling element
α_0	unloaded bearing contact angle
ψ_j	angular distance of j^{th} rolling element from the x-axis
$\{q\}_{bm}$	mean bearing displacement vector
$\{f\}_{bm}$	mean bearing load vector
Q_j	resultant normal load on the j^{th} rolling element
K_n	rolling element load – deflection stiffness constant
n	rolling element load – deflection exponent
Z	total number of rolling elements
z	number of loaded rolling elements
M_{bpm}	mean bearing moment about p = x or y direction
F_{bim}	mean bearing force in the i = x, y or z direction
$\{q\}_{ba}$	alternating bearing displacement vector
OEM	Original Equipment Manufacturer
REBM	Rolling Element Bearing Matrix

CHAPTER I

INTRODUCTION

Background

Tapered roller bearings are used for a number of applications including vehicle front wheels, differential and pinion configurations in drive axles, conveyor rolls, machine tool spindles and trailer wheels. This thesis examines the vibration effects of the tapered roller bearing present in the pinion shaft of the differential assembly of a heavy-duty truck.

During the drive axle operation, the ring gear exerts a thrust force of high magnitude on to the pinion shaft, and this force is countered by the tapered roller bearings. This axial force is then transmitted to the axle housing through the tapered roller bearing. A study has been made to analyze the bearing stiffness coefficients under pure axial conditions and also for radial load conditions with an axial preload.

Mathematical modeling of the tapered roller bearing involves numerous concerns because of its non-linear elastic behavior. This non-linearity is due to the Hertzian contact stresses and also the clearance between the rolling elements and the races. This thesis explores the validation of the mathematical model to determine the stiffness coefficients and examines the effectiveness of the stiffness matrix using an

experimental approach. The stiffness matrix has been examined under two load conditions, axial and radial. Variations of the stiffness coefficients based on the loading conditions have been studied.

Tapered roller bearings

Tapered roller bearings, because of their geometry, can carry heavy radial loads or thrust loads or a combination of both. The taper of the rollers, cup and the cone meet at a common apex on the bearing centerline. This results in true rolling motion of the rollers on the raceways. Each bearing consists of the cone, cup, cage and the rollers. The cage holds the rollers in place and does not carry any load. Two types of bearing loading may exist. The first is pure axial loading and the second type is the combined loading. This combined loading consists of a combination of radial and thrust loading. For a given taper angle, increasing the radial load will increase the induced thrust. For a constant radial load, increasing the taper angle will increase the thrust. [1]

Research objectives

The stiffness matrix of the bearing for pure axial loads and combined thrust and radial loading conditions were determined using an analytical model. From the results, the dominant stiffness coefficients were established. The axial and radial load deflection curves were plotted from the results.

An experimental fixture to measure the axial stiffness of the bearing was designed and manufactured. A second experimental fixture was designed to measure the radial stiffness of the bearing under radial load conditions with an axial preload. The axial preload was kept constant and the radial load varied from 4 KN up to 100 KN to verify the change in stiffness under high radial load conditions.

The results obtained from the experimental and the analytical data were compared with that of OEM (Original Equipment Manufacturer) data, REBM (Rolling Element Bearing Matrix) calculations, and ABAQUS model (Finite Element Analysis software).

CHAPTER II

LITERATURE SURVEY

Many papers have been published which describe the rolling element bearings as translational stiffness elements. There are not many papers pertaining to static measurement of bearing stiffness without any vibration. Walford and Stone [2] developed a method for measuring the radial stiffness of rolling element bearings under oscillating conditions. In their experiment, stiffness is measured as the ratio of the force on the bearings to the displacement across them. The paper also explains the effect of the inner / outer race temperature on bearing radial stiffness. The results concluded from their paper are:

Amplitude of force: With a fixed frequency of excitation and by increasing the amplitude of the force, the radial stiffness decreases.

Rotational speed: With a fixed excitation force amplitude and a fixed excitation frequency, the radial stiffness increases with rotational speed.

In 1989, Lin [3] established another test setup to measure the frequency response function at the plate (housing). Lin concludes from his experiment that increased radial preload increases the stiffness of the bearing at higher frequencies (over 1000 Hz). For the low frequency range (under 800 Hz), the vibration response is insensitive to the bearing preload. Kraus, Blech and Braun [4] present a method for the extraction

of rolling bearing characteristics (stiffness and damping) under operating conditions. An in situ measurement test stand was designed to determine the translational bearing stiffness from measured vibration spectra, in conjunction with the single degree-of-freedom system theory. The result concluded was that by increasing the bearing preload, the stiffness increases in both the radial and axial directions. Further, damping decreases radially and increases in the axial direction with an increase in preload. Some of the other vibration measurement techniques were performed by Su and Lin [5], who investigated the vibrations of a tapered roller bearing fitted into a housing. They showed that tapered roller bearing vibrations are effected by geometrical imperfections due to manufacturing errors. Ohta and Sugimoto [6] performed an experimental setup to determine the vibration characteristics of the tapered roller bearings.

T.C. Lim and R. Singh have developed a bearing model of dimension six which demonstrated a coupling between the shaft bending motion and the flexural motion of the casing plate [8]. They have developed a numerical scheme which involves solution of non-linear algebraic equations for the estimation of stiffness coefficients given the mean bearing load vector. They have also performed vibration transmission analyses for a generic shaft-bearing-plate-mount system [9], by extending the bearing stiffness formulation presented in their previous paper [8]. REBM, a mathematical computation program, developed by Dr. Lim can be used to determine the stiffness matrix of ball and roller type bearing. It has been explained in detail in Chapter III.

CHAPTER III

ROLLING ELEMENT BEARING MATRIX (REBM) PROGRAM

REBM is a bearing stiffness matrix calculation program developed by Prof. Teik C. Lim. The software uses the mathematical model developed by T.C. Lim and R. Singh in their papers [8, 9]. They develop separate formulations for ball and roller type bearings depending upon the contact between the inner race, rolling elements and outer race when loaded. In the derivation of the bearing stiffness matrix, the basic load-deflection relation for each elastic rolling element is defined by the Hertzian contact stress theory. The load experienced by each rolling element is described by its relative location in the bearing raceway. Further, it has also been assumed that the angular position of each rolling element relative to one another is always maintained due to rigid cages and pin retainers.

The mean applied loads at the shaft and the bearing preloads generate the mean bearing displacements $\{q\}_{bm}$ and loads $\{f\}_{bm}$. The resultant elastic deformation of the j[th] rolling element located at an angle ψ_j from the x-axis is given by:

$$\delta_R(\psi_j) = \begin{cases} (\delta)_{rj}\cos\alpha_j + (\delta)_{zj}\sin\alpha_j, & \delta_{Rj} > 0 \\ 0, & \delta_{Rj} \le 0 \end{cases} \qquad (1)$$

where,

$(\delta)_{rj}$ effective j[th] rolling element displacement in the radial direction

$(\delta)_{zj}$ effective j[th] rolling element displacement in the axial direction

ψ_j angular distance of j[th] rolling element from the x-axis

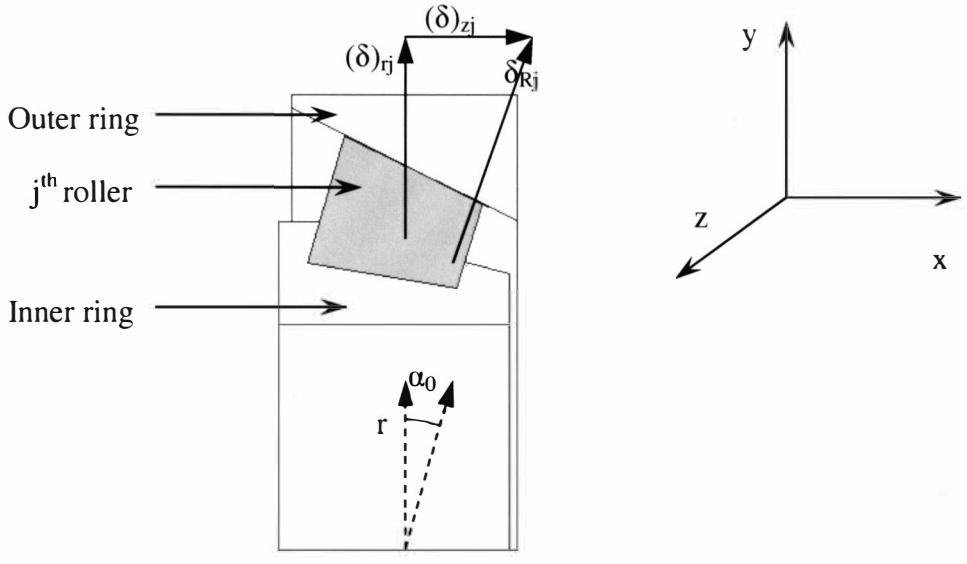

Figure 3.1: Elastic deformation of rolling element for constant contact angle

This equation together with the Hertzian contact stress principle [1] yields the load deflection relationship for a single rolling element:

$$Q_j = K_n \delta_j^n \tag{2}$$

Here, Q_j is the resultant normal load on the rolling element and K_n is the effective stiffness constant for the inner race-rolling element-outer race contacts and is a function of the bearing geometry and material properties.

The resultant bearing mean load vector and the bearing displacement vectors are related for all of the loaded rolling elements and this leads to the bearing moments and forces:

$$\begin{Bmatrix} M_{bxm} \\ M_{bym} \\ M_{bzm} \end{Bmatrix} = K_n \sin\alpha_0 \sum_j^z r_j \left\{ (\delta)_{rj} \cos\alpha_0 + (\delta)_{zj} \sin\alpha_0 \right\}^n \begin{Bmatrix} \sin\psi_j \\ -\cos\psi_j \\ 0 \end{Bmatrix}, \tag{3}$$

$$\begin{Bmatrix} F_{bxm} \\ F_{bym} \\ F_{bzm} \end{Bmatrix} = K_n \sum_j^z \left\{ (\delta)_{rj} \cos\alpha_0 + (\delta)_{zj} \sin\alpha_0 \right\}^n \begin{Bmatrix} \cos\alpha_0 \cos\psi_j \\ \cos\alpha_0 \sin\psi_j \\ \sin\alpha_0 \end{Bmatrix} \tag{4}$$

The symmetric bearing stiffness matrix $[K]_{bm}$ of dimension six has been defined from equations (3) and (4) and by assuming that $\{q\}_{ba} \langle\langle \{q\}_{bm}$

$$[K]_{bm} = \begin{bmatrix} \partial F_{bim}/\partial\delta_{jm} & \partial F_{bim}/\partial\beta_{jm} \\ \partial M_{bim}/\partial\delta_{jm} & -\partial M_{bim}/\partial\beta_{jm} \end{bmatrix} \qquad i, j = x, y, z \tag{5}$$

where,

$\{q\}_{ba}$ alternating bearing displacement vector
$\{q\}_{bm}$ mean bearing displacement vector

Complete derivation of the mathematical model has been given in [1].

By entering the bearing geometry and by specifying the radial and axial displacements, the REBM software computes the bearing stiffness matrix, angular position of the rollers and also the number of rollers in contact. The stiffness matrix calculated by the software is of the form,

$$[K]=\begin{bmatrix} K_{xx} & K_{xy} & K_{xz} & K_{x\theta_x} & K_{x\theta_y} & K_{x\theta_z} \\ K_{yx} & K_{yy} & K_{yz} & K_{y\theta_x} & K_{y\theta_y} & K_{y\theta_z} \\ K_{zx} & K_{zy} & K_{zz} & K_{z\theta_x} & K_{z\theta_y} & K_{z\theta_z} \\ K_{\theta_x x} & K_{\theta_x y} & K_{\theta_x z} & K_{\theta_x\theta_x} & K_{\theta_x\theta_y} & K_{\theta_x\theta_z} \\ K_{\theta_y x} & K_{\theta_y y} & K_{\theta_y z} & K_{\theta_y\theta_x} & K_{\theta_y\theta_y} & K_{\theta_y\theta_z} \\ K_{\theta_z x} & K_{\theta_z y} & K_{\theta_z z} & K_{\theta_z\theta_x} & K_{\theta_z\theta_y} & K_{\theta_z\theta_z} \end{bmatrix}$$

where,

K_{xx}, K_{yy} and K_{zz} are the translational stiffness coefficients.

The accuracy of the REBM software, in computing bearing stiffness, has also been verified by comparing it with other analytical and experimental values. The procedure for the operation of the software has been detailed in Appendix A. Figure 3.2 shows the geometric and effective centers of the bearing. REBM uses the geometric center for its calculations.

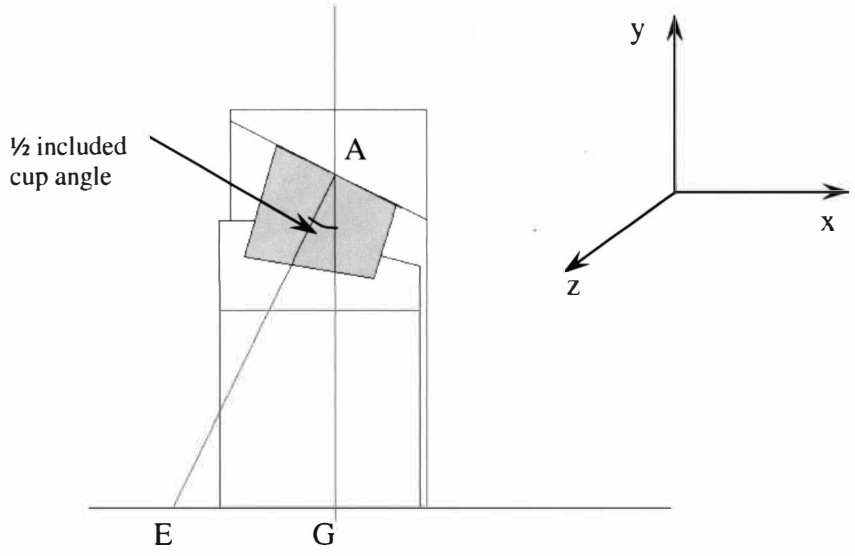

Figure 3.2: Cross-section of the bearing showing the geometric center (G) and effective center (E)

Dominant stiffness coefficients

Dominant stiffness coefficients have been identified by choosing the coefficients with high magnitudes (10^6 times higher than the next significant coefficient). The dominant stiffness coefficients were calculated for three different conditions,

1.) Axial load only

2.) 180 degree load zone

3.) Combined radial and axial loading

Based on the bearing stiffness matrix generated, the stiffness coefficients that of high magnitude were identified. They are K_{xx}, K_{yy}, K_{zz}, K_{RxRx}, K_{RyRy}, K_{xRy}, K_{RyX}, K_{RxY}, and K_{yRx}. Here, K_{xx}, K_{yy} and K_{zz} are the translational stiffness coefficients. K_{RxRx} and K_{RyRy} are the rotational stiffness coefficients. K_{xRy}, K_{RyX}, K_{RxY}, and K_{yRx} are the off-diagonal terms in the stiffness matrix. For all calculations, "z" is the axis of the bearing. This thesis examines the variation and correlation of the translational stiffness coefficients with other viable numerical and experimental models. The axial load condition deals with the case where the bearing is subject to axial load only. Table 3.1 shows the magnitude of the dominant stiffness coefficients under pure axial load conditions.

Axial load	Kxx	Kyy	Kzz	K RxRx	K RyRy	K xRy	K RyX	K RxY	K yRx
N	MN/mm	MN/mm	MN/mm	GN-mm/rad	GN-mm/rad	GN/rad	GN/rad	GN/rad	GN/rad
4000	3.84	3.84	2.8	2.44	2.44	-0.094	-0.094	0.094	0.094
20000	4.67	4.51	3.29	2.87	2.87	-0.11	-0.11	0.11	0.11
40000	4.83	4.83	3.53	3.07	3.07	-0.118	-0.118	0.118	0.118
60000	5.03	5.03	3.67	3.2	3.2	-0.123	-0.123	0.123	0.123
85000	5.21	5.21	3.8	3.31	3.31	-0.127	-0.127	0.127	0.127
98000	5.29	5.29	3.86	3.36	3.36	-0.129	-0.129	0.129	0.129

Table 3.1: Dominant stiffness coefficients during pure axial load condition

During the pure axial load condition, axial load on the bearing was given from 4000 N to 98000 N. Figure 3.2 shows that the stiffness increases gradually as the load was applied axially. The increase in the axial stiffness during low loads (less than 20 KN) was found to be greater than that at high loads.

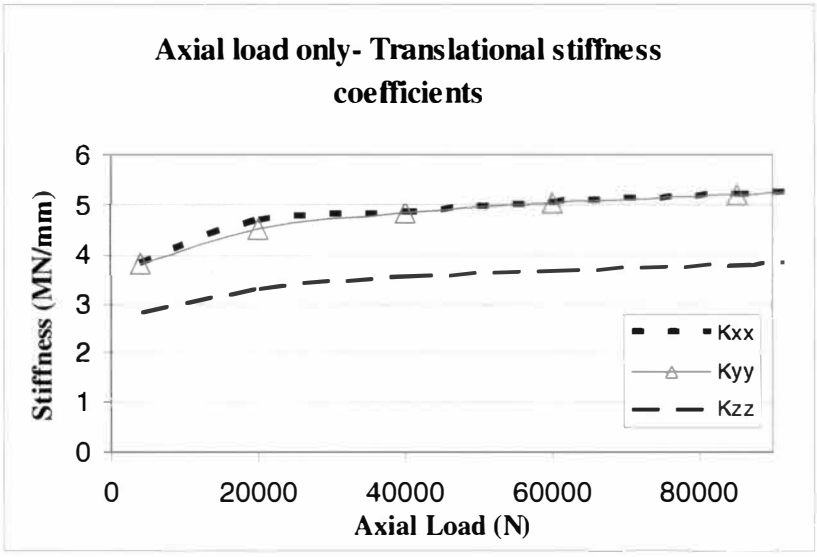

Figure 3.3: Variation of translational stiffness coefficients given pure axial load

For the 180 degree load zone, the load was applied radially in 'y' direction only. The axial load was induced because of the taper of the raceways and was not applied externally. The variation of the translational stiffness coefficients can be seen in Figure 3.3. Table 3.2 shows the magnitude of the dominant stiffness coefficients on a 180 degree load conditions.

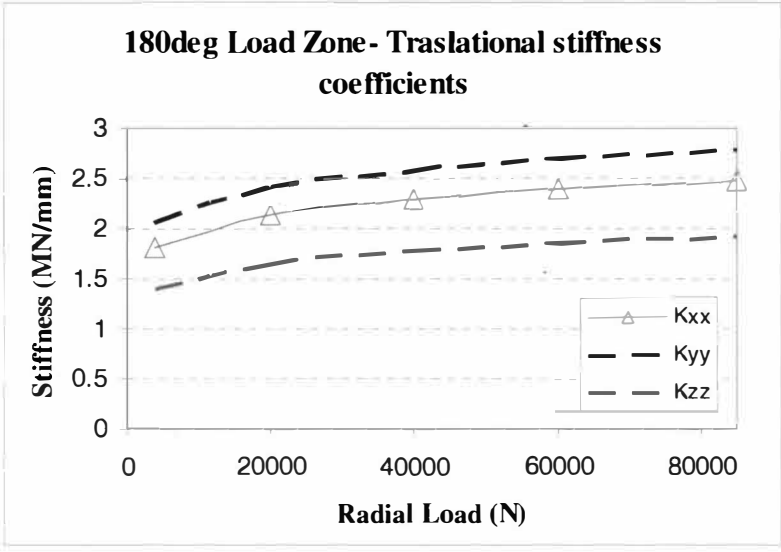

Figure 3.4: Variation of translational stiffness coefficients on a 180 degree load zone

Radial load	Kxx	Kyy	Kzz	K RxRx	K RyRy	K xRy	K RyX	K RxY	K yRx
N	MN/mm	MN/mm	MN/mm	GN-mm/rad	GN-mm/rad	GN/rad	GN/rad	GN/rad	GN/rad
4000	1.83	2.06	1.41	1.31	1.16	-0.045	-0.045	0.05	0.05
20000	2.15	2.42	1.66	1.53	1.37	-0.052	-0.052	0.059	0.059
40000	2.3	2.59	1.78	1.65	1.46	-0.056	-0.056	0.063	0.063
60000	2.4	2.7	1.86	1.72	1.52	-0.058	-0.058	0.066	0.066
85000	2.48	2.79	1.92	1.78	1.58	-0.061	-0.061	0.068	0.068

Table 3.2: Variation of translational stiffness coefficients on a 180 degree load zone

The third condition is the combined loading condition such that the rollers always maintain a 360 degree loading zone. This is accomplished by applying a constant axial load of 98000 N and the radial load is applied from 4 KN to 85 KN. Figure 3.4 shows that the stiffness of the bearing remains constant up to a load of 60 KN and

then decreases slightly. The pure axial loading and the combined loading conditions have been verified experimentally and are explained in the forthcoming chapters.

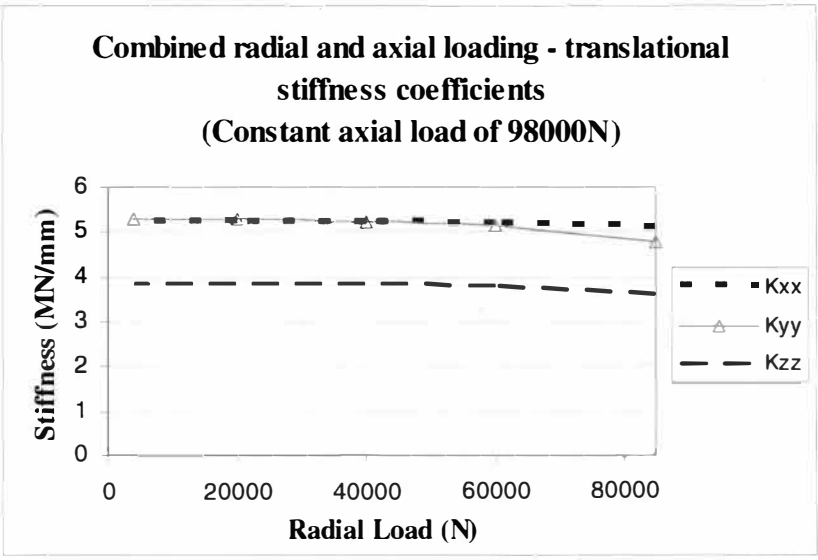

Figure 3.5: Variation of translational stiffness coefficients on combined axial and radial loading

Table 3.3 shows the magnitude of the dominant stiffness coefficients during radial load conditions with an axial preload. The axial load was applied with a constant magnitude of 98000 N.

Radial load	Kxx	Kyy	Kzz	K RxRx	K RyRy	K xRy	K RyX	K RxY	K yRx
N	MN/mm	MN/mm	MN/mm	GN-mm/rad	GN-mm/rad	GN/rad	GN/rad	GN/rad	GN/rad
85000	5.17	4.79	3.63	3.05	3.29	-0.126	-0.126	0.117	0.117
60000	5.25	5.17	3.79	3.29	3.34	-0.128	-0.128	0.126	0.126
40000	5.27	5.24	3.83	3.33	3.35	-0.129	-0.129	0.128	0.128
20000	5.28	5.28	3.85	3.35	3.36	-0.129	-0.129	0.129	0.129
4000	5.29	5.29	3.86	3.36	3.36	-0.129	-0.129	0.129	0.129

Table 3.3: Variation of translational stiffness coefficients on combined axial and radial loading

CHAPTER IV

FINITE ELEMENT ANALYSIS

Pro/E model

A parametric solid model of the tapered roller bearing was created using Pro/E. Because of the parametric nature of the model, the model regenerates itself for any bearing dimensions entered. The dimensions to be entered are the cone bore diameter, the cup outside diameter, the cup and cone angles. Figure 4.1 shows the cross-sectional view of the tapered roller bearing. The Pro/E model can be used with any finite element analysis software to compute the bearing stiffness. Since ABAQUS had the capability of creating the model of the tapered roller bearing within itself, the solid model created using Pro/E was not used. But it can be used to perform finite element analysis using other software like ANSYS.

Figure 4.1 shows the cross-sectional view of the tapered roller bearing with the dimensions that need to be entered. Here'd' is the cone bore diameter, 'D' is the cup outside diameter, 'a' and 'b' are ½ included cone and cup angles respectively.

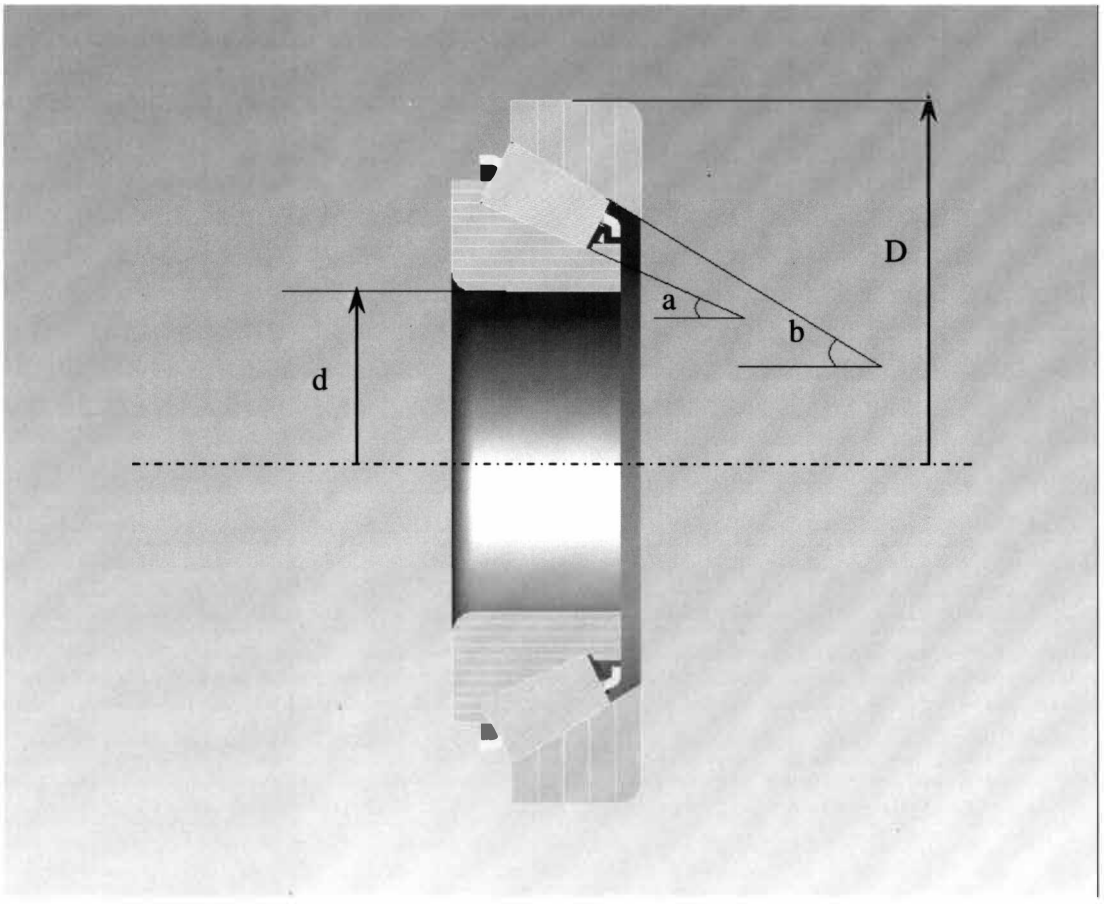

Figure 4.1: Cross-sectional view of the tapered roller bearing

Figure 4.2 shows the solid model of the bearing cone with the cage. The cage is present to prevent rigid-body motion of the rollers.

Figure 4.2: Solid model of the bearing cone with the cage

ABAQUS model

The ABAQUS model is a non-linear contact model which has the inner, outer races and tapered rollers modeled as deformable bodies. The outside of the cup and the inside of the cone are tied to rigid bodies. The model has contact elements between rollers and races and also includes a preload. The cage present in the bearing was simulated by boundary constraints to prevent rigid body motion of rollers. The ABAQUS super element technique was used to generate a 6 DOF global stiffness

matrix for the bearing. The model has been used as a comparison criterion in this thesis. Table 4.1 shows the deflection of the bearing for various axial loads.

ABAQUS model	
Load	Deflection
KN	mm
4	0.001398
20	0.006989
40	0.013977
60	0.020963
85	0.029693
98	0.034232

Table 4.1: Load deflection values generated from the ABAQUS model

CHAPTER V

SENSORS AND FIXTURES FOR STIFFNESS MEASUREMENT

Inductive displacement sensor

A sensor was required to perform data acquisition since the noise emanating from the Material Testing System (MTS) of the test lab was measured to have peak to peak value of 0.5 mm. Since the measurements were between 0.007 – 0.02 mm, a sensor with higher resolution and signal to noise ratio was required. Inductive sensors detect the proximity of a metal object by gauging the effect the metal target has upon a magnetic field emanating from the sensor. Inductive sensors are very accurate, highly repeatable, non-contact devices that employ solid state technology and exhibit very low hysteresis. Inductive sensors are also one of the most expensive types of discrete sensors. The specific inductive displacement sensor, used for measurement, has a resolution of 0.4 μm within a range of 0 – 2 mm with a linearity of ± 0.3% full scale. The analog output measured from the sensor with a ferrite core attached around the wires, to prevent noise from surrounding equipment, had a peak to peak noise level of 0.0056 mm. The digital output also has a sampling rate of 40,000 samples max. / sec.

Experimental fixture for axial load test

The fixture designed for the axial load - deflection test has been shown in Figure 5.1. The three main components are:

1.) Shaft

2.) Housing

3.) Tapered roller bearing

The shaft has two diameters. The smaller diameter was specified to have a sliding fit to the cone of the bearing. The larger diameter has a shoulder to push against the cone of the bearing when applying axial load. The housing also has two holes to tap the cup out of the housing, so that the test can be performed for other bearings. The sensor is inserted inside the housing and the distance from the face of the sensor head to the face of the shaft was kept to be 2 mm. This was accomplished with the help of a gage block. The sensor was held in place with the help of a jam nut. Load was applied from 100 N to 96 KN. The load-deflection curve for this test is shown in Chapter VI. A certain degree of non-linearity existed at low loads (below 10 KN). This was due to the clearance, between the shaft and the inner diameter of the bearing cone, to allow the shaft to slide in and out of the bearing easily.

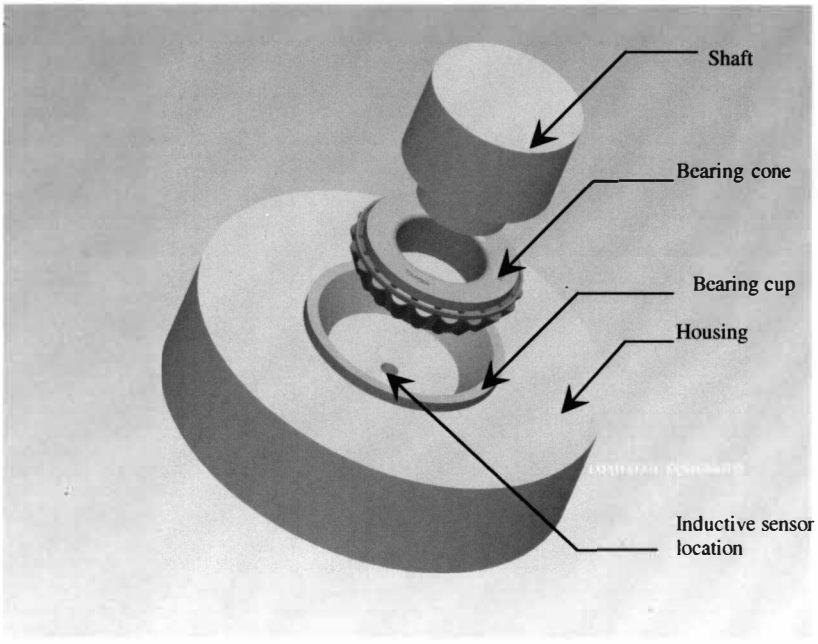

Figure 5.1: Exploded view of the axial load test fixture showing various components

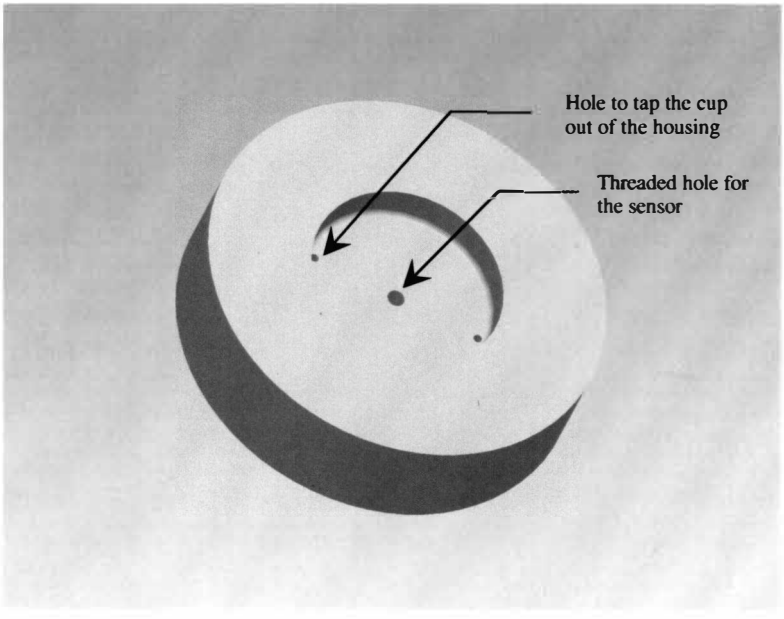

Figure 5.2: Solid model of the housing used for the axial load test

The housing has a slot on one side for the sensor wire to be pulled out. The housing is also provided with two holes to tap the press-fit bearing cup out from the housing. This facilitates the test to be carried out for different bearings.

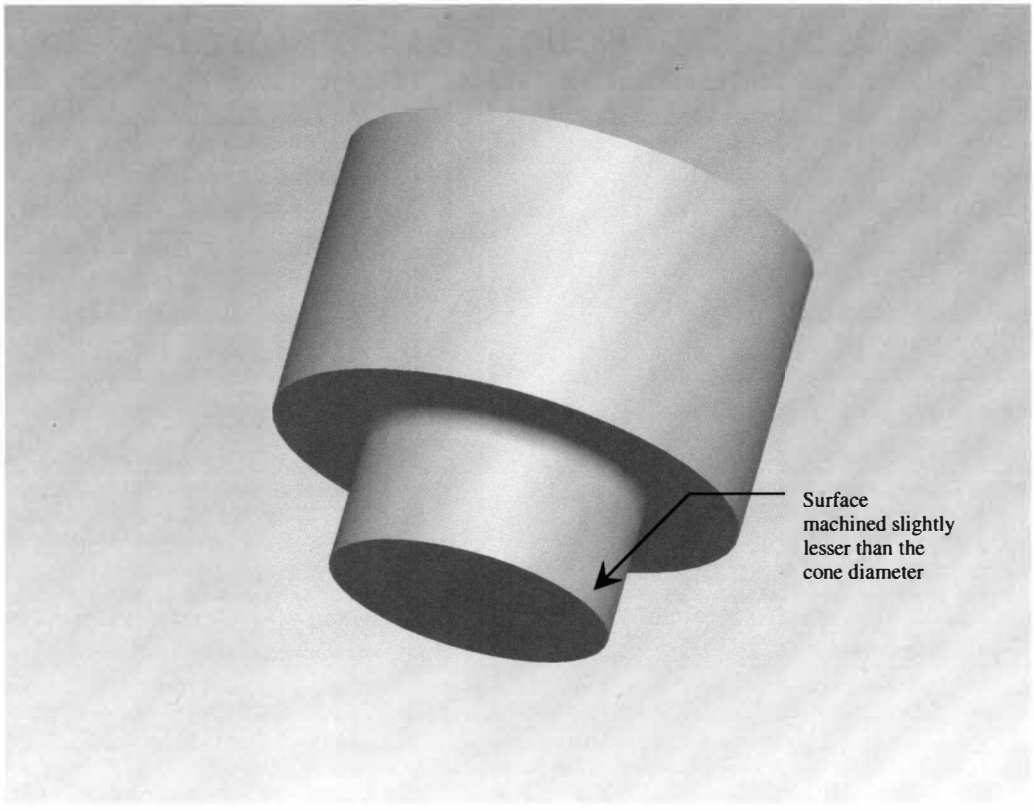

Figure 5.3: Solid model of the shaft used for the axial load test

The larger diameter of the shaft pushes against the bearing cone. The shaft has been designed this way, to apply an axial load throughout the surface of the bearing cone. The shaft and the housing have been made thicker to have increased stiffness. Figure 5.4 shows the axial load test fixture. The axial load was applied on the test fixture by the Material Test System. Figure 5.5 shows the various components of the axial load test fixture. The location of the inductive displacement sensor is also shown.

Figure 5.4: Axial test fixture in loaded condition

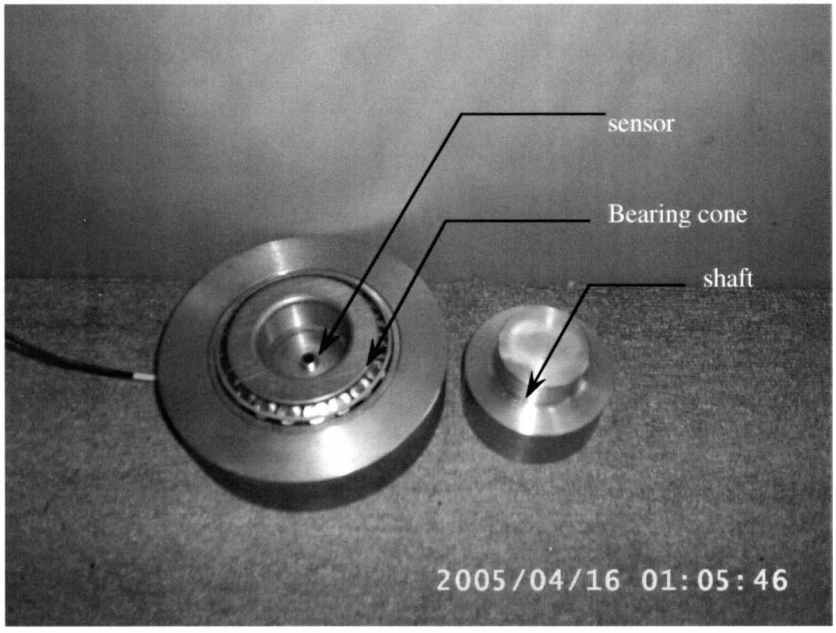

Figure 5.5: Components of the axial test fixture with the sensor

Experimental fixture for radial load test

The experimental fixture designed for the radial load - deflection test has been explained below. The radial load – deflection test has been conducted by applying an axial preload and by varying the radial load. The radial load has been applied with the help of a Material Testing System (MTS). The major components are:

1.) Housing
2.) Shaft
3.) Upper fixture
4.) Outer flange
5.) Nut
6.) Bolts
7.) Tapered roller bearings

The radial test fixture has been designed to test either a single bearing or a pair of bearings.

Two bearing test fixture

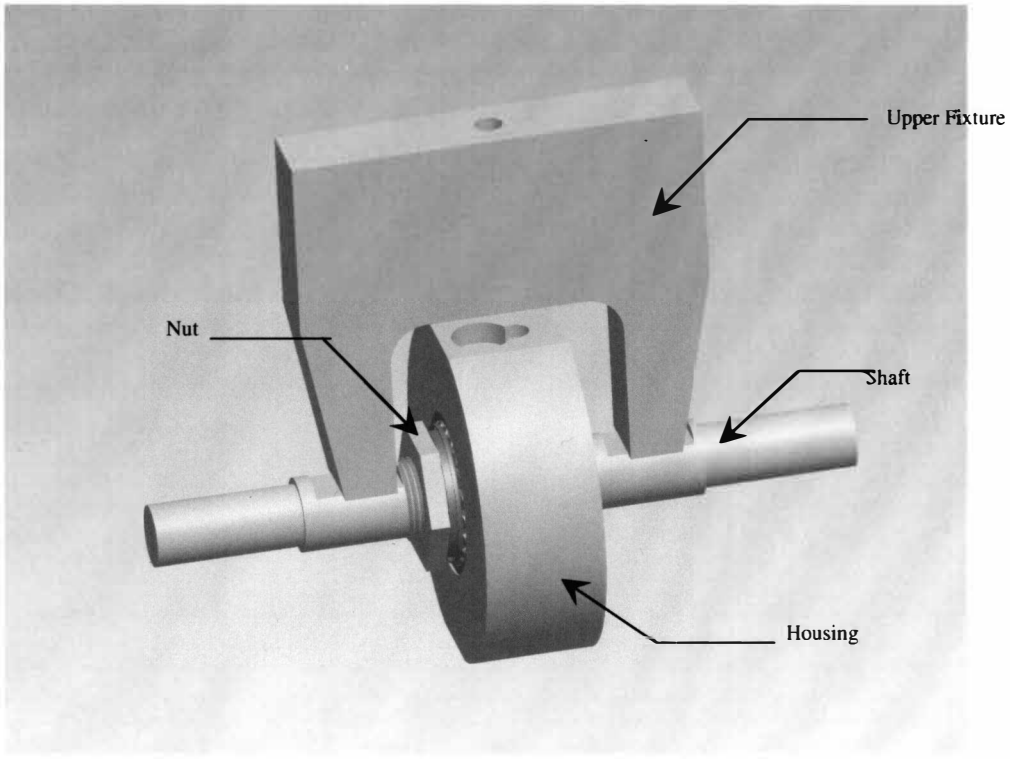

Figure 5.6: Assembled view of the radial load test fixture to test two bearings

Figure 5.9 shows the radial test fixture used to measure the displacement across two bearings. The lock nut was used to apply the axial preload on the bearings. The sensor threaded to the housing senses the displacement across the bearings by the relative movement of the probe. The sensor location has been shown in Figure 5.10. The wires from the sensor were connected to a display controller which displayed the displacement across the bearings.

The strain gage wire can also be seen in Figure 5.10. The wire was connected to a strain indicator which displayed the measured strain across the shaft. From the strain on the shaft, the axial load on the bearings was calculated. This has been detailed in Chapter VI.

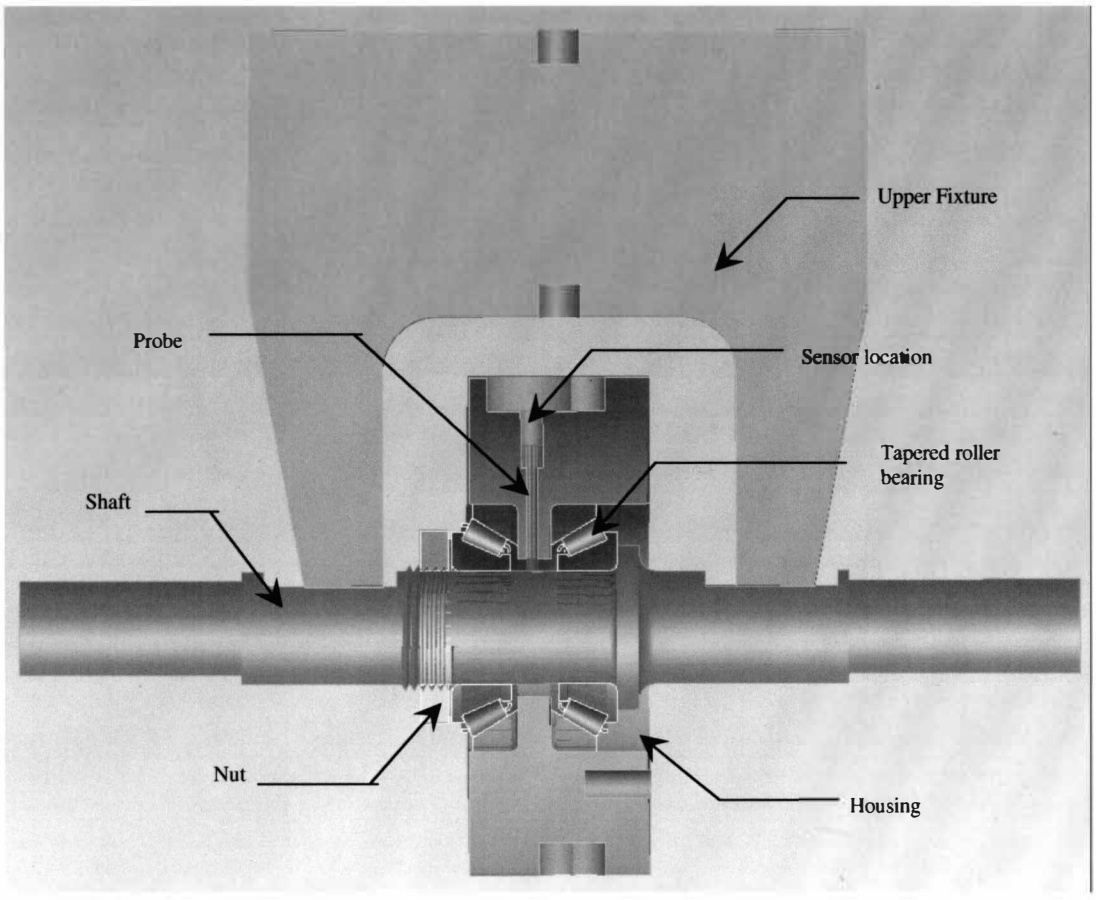

Figure 5.7: Cross sectional view of the radial test fixture

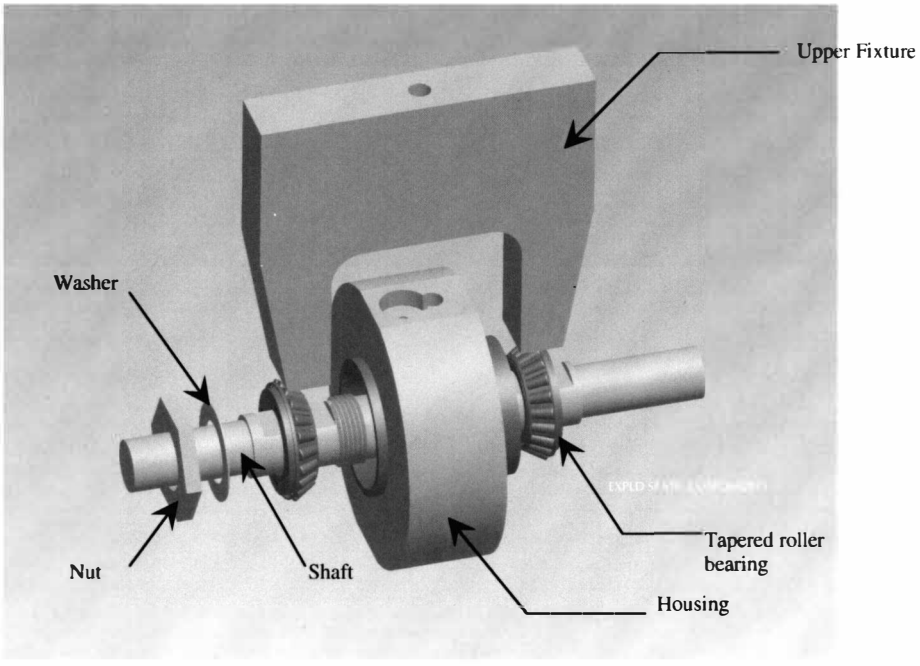

Figure 5.8: Exploded view of the radial test fixture showing various components

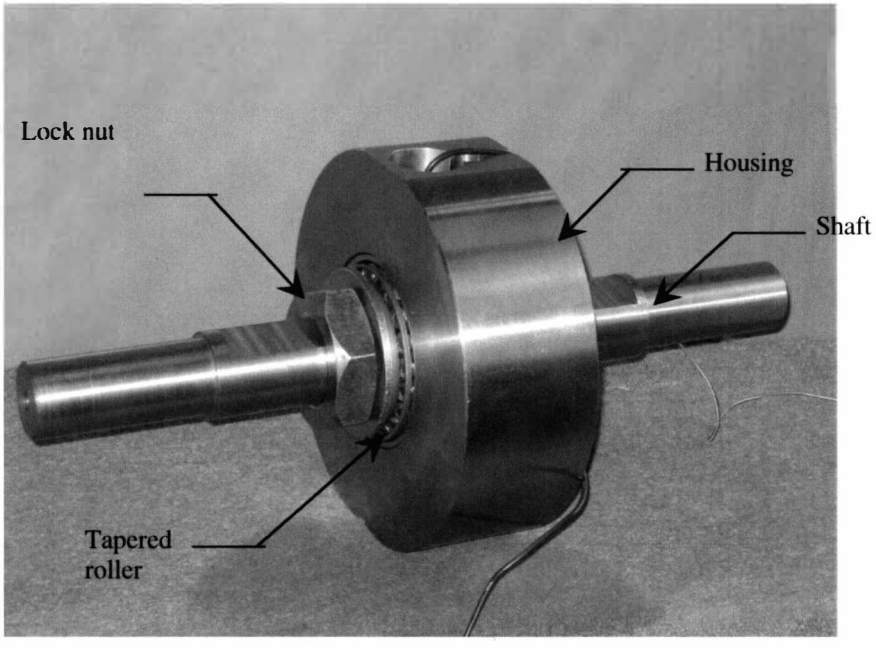

Figure 5.9: Radial test fixture to measure the displacement across two bearings

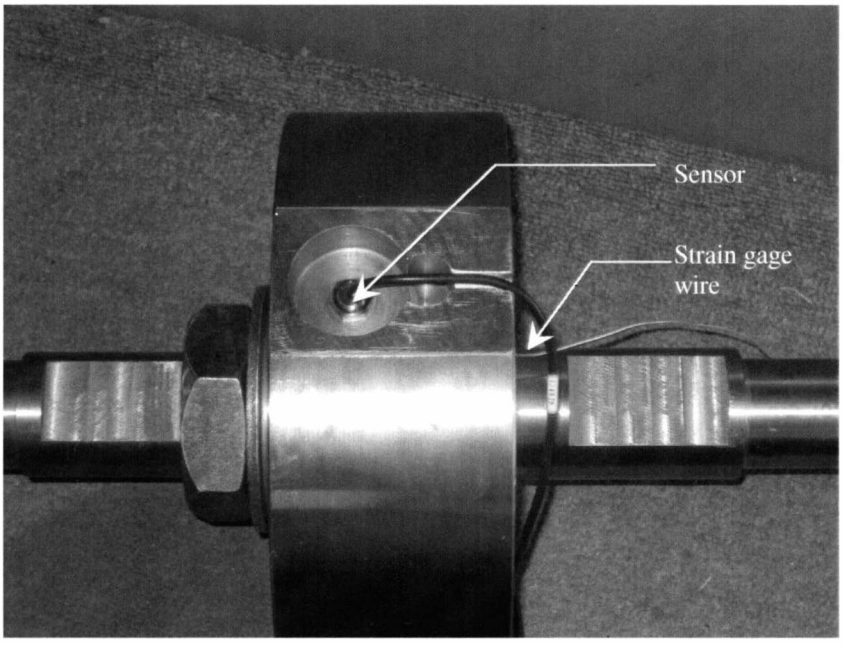

Figure 5.10: Radial test fixture showing the sensor location

Housing

The housing has protrusion cuts on either side to include the tapered roller bearings. On one side, the housing has three holes, drilled and equally spaced for the nuts. The radial test fixture was designed with the flexibility to test either a pair of bearings or just one bearing at a given instant. The housing has flat surfaces machined on the top and bottom for the housing not to lose balance, when radial load was applied through the MTS (Material Testing System) machine. The "kidney-shaped" holes at the top and bottom of the housing were used to locate the bearing centrally, when applying the radial load through the Material Testing System (MTS). The protrusion cuts on

the sides of the housing were rounded so that the bearing was a press-fit to the housing. The housing has slots present on the inside to facilitate easy removal of the bearings, with the help of a bearing-puller. The housing also has a threaded hole for the sensor. The threaded hole also holds a probe in place which rests on the surface of the shaft. The relative displacement of the probe caused by the movement of the shaft is sensed by the displacement sensor.

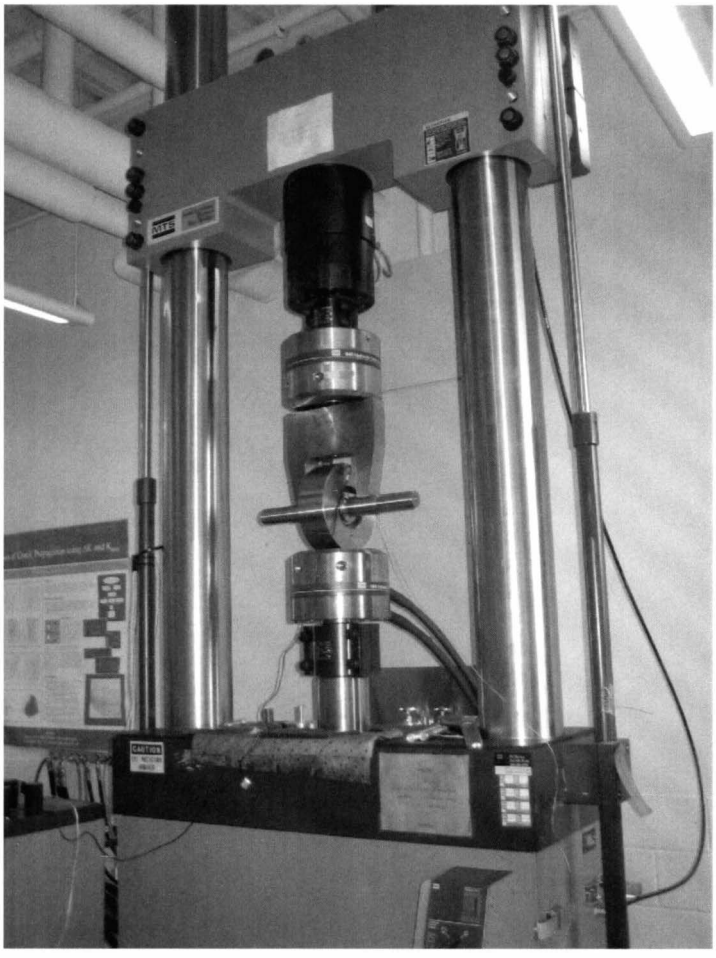

Figure 5.11: Radial load being applied on the test fixture

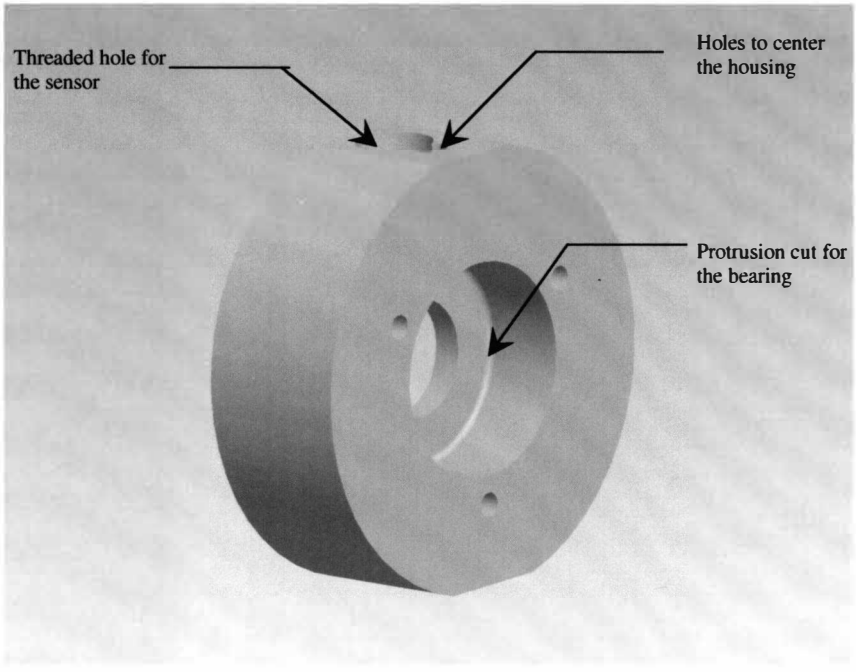

Figure 5.12: Solid model of the housing used in the radial load – deflection test

Shaft

The shaft has been manufactured of mild steel. One of the bearing rests against the shoulder of the shaft. Another bearing slides through the shaft and axial preload was applied with the help of a nut. The two flats present on the shaft have been machined for the upper fixture to apply radial load on the bearings. The step on the bearing was included for future vibration testing wherein weights can be added to the shaft. The shaft also has a strain gage glued on its surface between the two bearings shown in Figure 5.14. The strain gage was offset 5mm from the bearing centerline so that it did not cause interference with the probe. The axial preload applied by the nut was sensed by the strain gage and measured using a strain indicator.

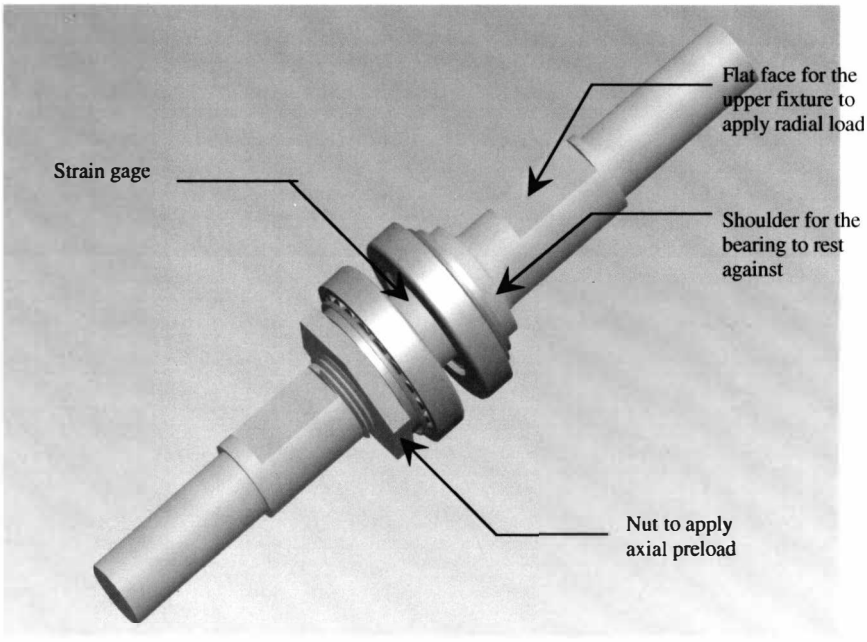

Figure 5.13: Solid model of the shaft used in the radial load – deflection test

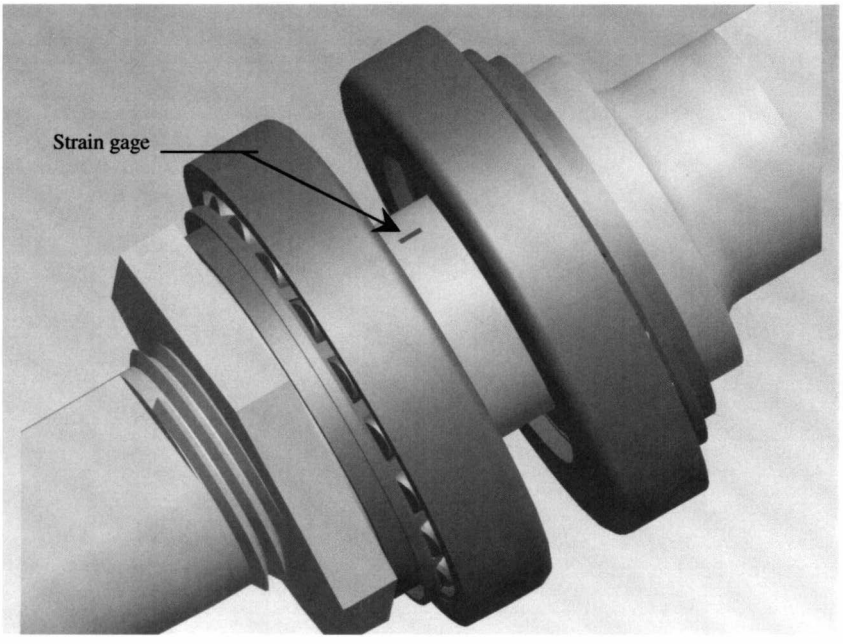

Figure 5.14: Location of the strain gage on the shaft

Single bearing test fixture

The single bearing test fixture can be used instead of the 2 bearing test fixture, if the resolution of the sensor used is not high enough to measure the deflection of two bearings. The outer flange was used in this case, to give the axial preload.

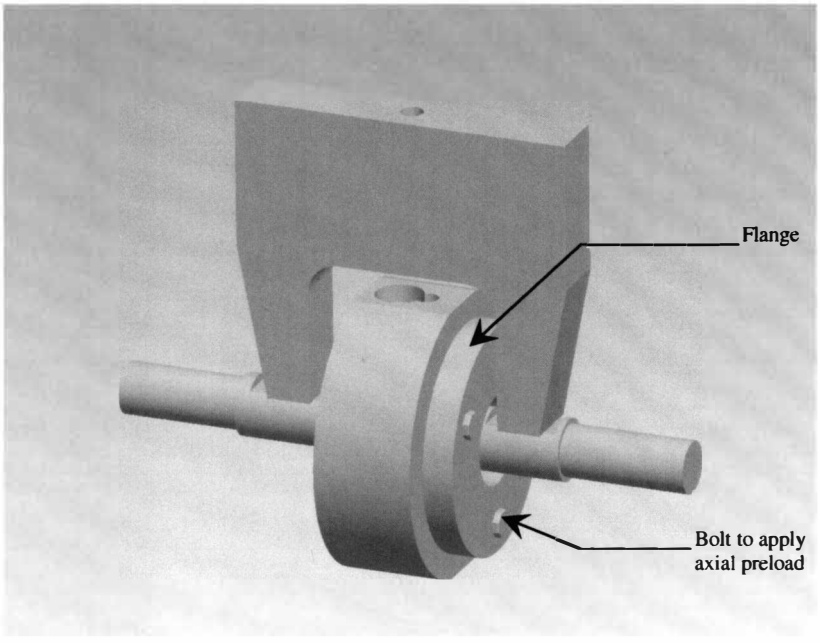

Figure 5.15: Radial load test fixture to test a single bearing

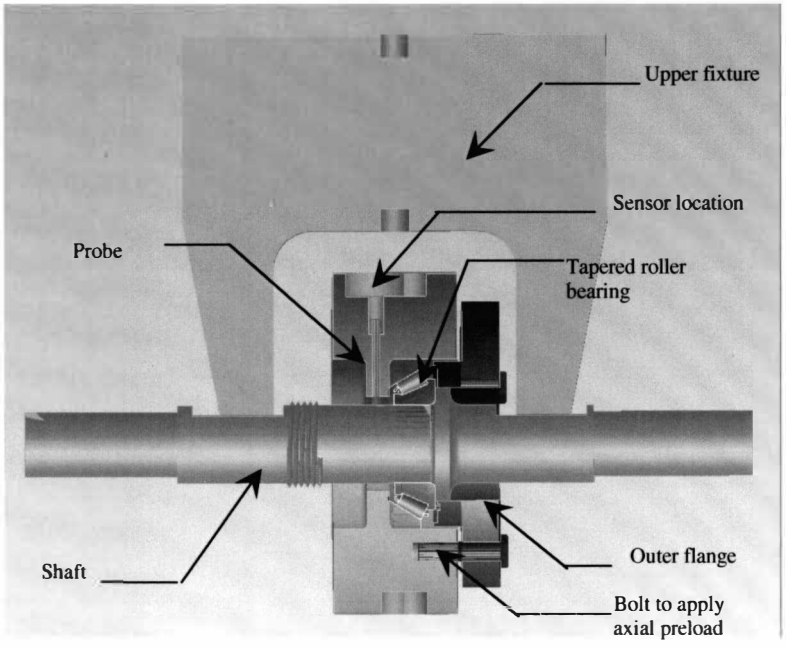

Figure 5.16: Cross-section of the radial test fixture to test a single bearing

Outer flange

The outer flange was used only when measuring the stiffness of one bearing. The flange will press against the cone of the bearing when applying the axial preload. The axial preload applied through the bolts was measured using bolt sensors. The flange has three grooves equally spaced at an angle of 120 degrees. The grooves are present to hold three steel balls in place. When applying radial preload, the presence of the steel balls will produce a rolling motion which would minimize the friction between the cone and flange surfaces. The steel balls, through the flange will supply a reaction force to the thrust load induced by the applied radial load, due to the taper of the rollers. The flange was hardened to minimize ball indentations.

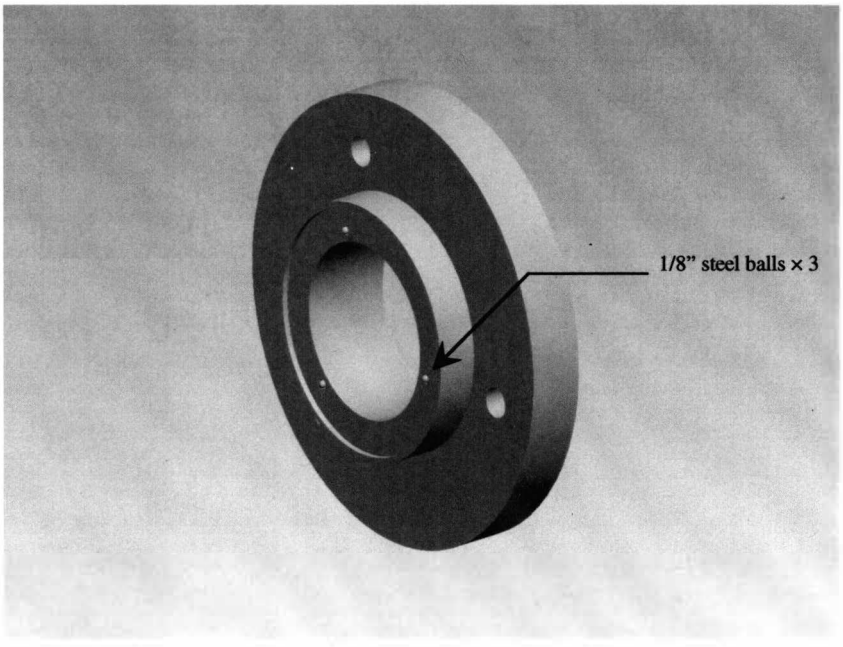

Figure 5.17: Solid model of the outer flange used in the radial load – deflection test

CHAPTER VI

EXPERIMENTAL STIFFNESS AND MEASUREMENT RESULTS

Axial load-deflection test (Pure axial loading)

The specific bearing used for the analysis has been detailed below

Series : 55000

Cone : 55200C

Cup : 55437

Results and explanation:

The bearing was press-fit into the housing and the load was applied axially through the MTS machine. The inductive displacement sensor was threaded into the housing. The distance between the sensor head and the shaft face was adjusted to be less than 2 mm, which is the range of the sensor. Load was then applied by the MTS machine and the displacement was measured directly from the controller display. Since the noise generated from the MTS machine (0.5 mm) was greater then the displacement of the bearing, the sensor had to be used for measurement purposes. The inductive displacement sensor was chosen because of the non-contact displacement measurement technique, robustness, small size and high resolution.

The experiment was performed for three different bearings of same type as shown in Table 6.1. Results show that the axial stiffness of the bearings experimentally tested, were lower than that shown by the other three approaches. This is due to the fact, that the shaft was made slightly smaller than the bearing cone to facilitate easy removal and also to test other bearings. The clearance between the shaft and the bearing cone accounted for some amount of deflection, when load was applied axially on the shaft.

TRIAL 1		**TRIAL 2**		**TRIAL 3**		**Average of 3 trials**	
Load	Deflection	Load	Deflection	Load	Deflection	Load	Deflection
KN	mm	KN	mm	KN	mm	KN	mm
4	0.003483	4	0.003289	4	0.003587	4	0.003453
20	0.017414	20	0.016445	20	0.017935	20	0.017265
40	0.034828	40	0.032890	40	0.035871	40	0.034530
60	0.052242	60	0.049335	60	0.053806	60	0.051794
85	0.074009	85	0.069891	85	0.076226	85	0.073375
98	0.085328	98	0.080580	98	0.087884	98	0.084597

Table 6.1: Axial load deflection values measure for 3 bearings

The load deflection curves generated in Figure 6.1 show that the bearing deflects more during the experimental measurement, when compared with other analytical models.

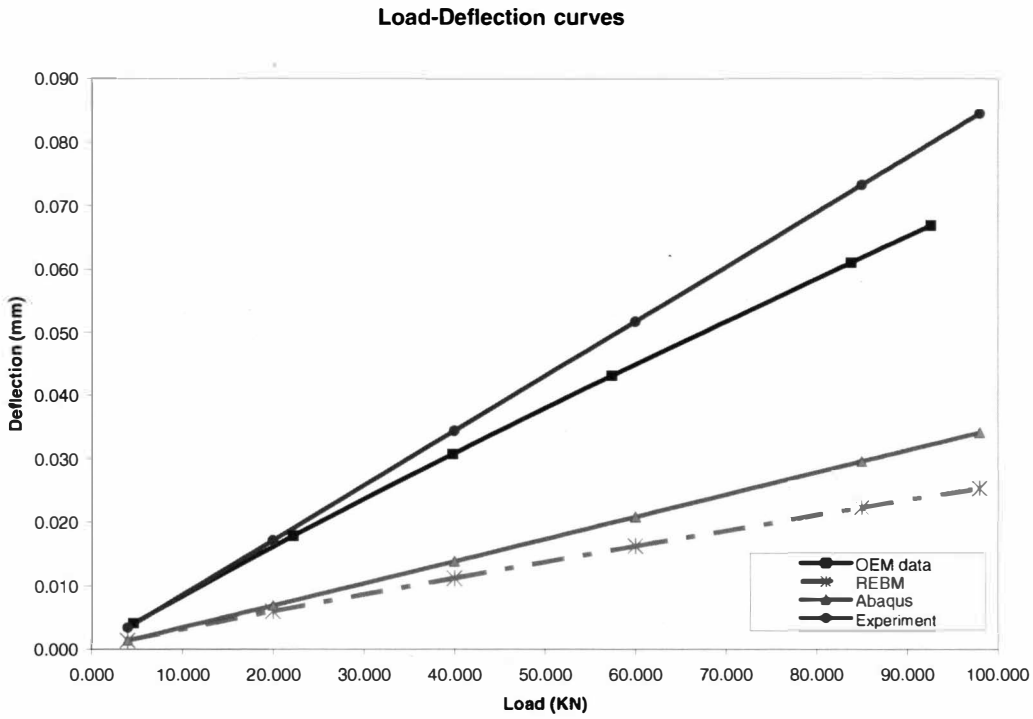

Fig 6.1: Comparison of the axial load deflection curves for different methods

The results from the REBM software are also tabulated in Table 6.1. The axial stiffness in this case is found to increase with the axial loading. The ABAQUS model shows an axial stiffness value that remains constant with increase in axial load. The variation in the axial stiffness between the four cases has been shown in Figure 6.2.

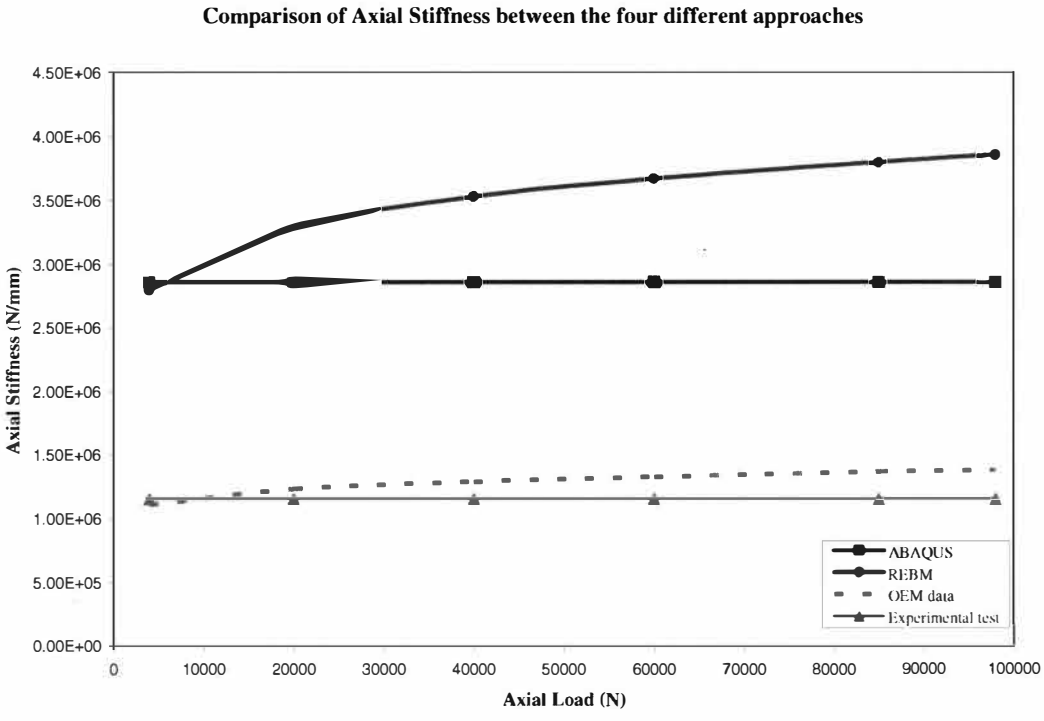

Fig 6.2: Comparison of axial stiffness coefficients for different methods

Repeatability of the axial load test

A study was also done on the repeatability of the test and also of the bearing. Figure 6.3 shows the load – deflection test performed on 1 bearing. At loads below 30 KN, non-linearity exists. This is due to the fact that the shaft was made slightly smaller than the bearing cone, to facilitate easy removal and also to test other bearings. When load was applied axially on the shaft, the clearance between the shaft and the bearing cone accounted for some amount of deflection. To eliminate this non-linearity, the curves have been offset. The new plots are shown in Figure 6.4. The load – deflection

test on 3 bearings have also been shown in Figure 6.5. These results show that the test is repeatable.

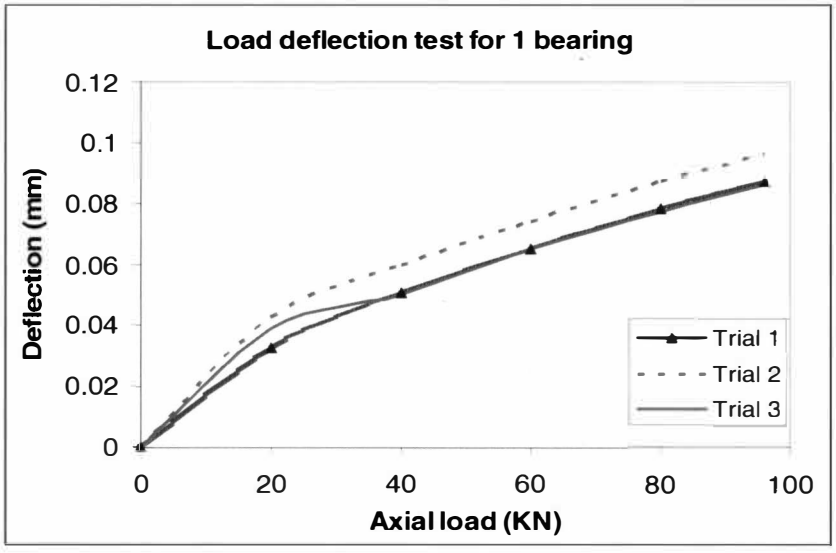

Figure 6.3: Load – deflection curve showing non-linearity at lesser loads

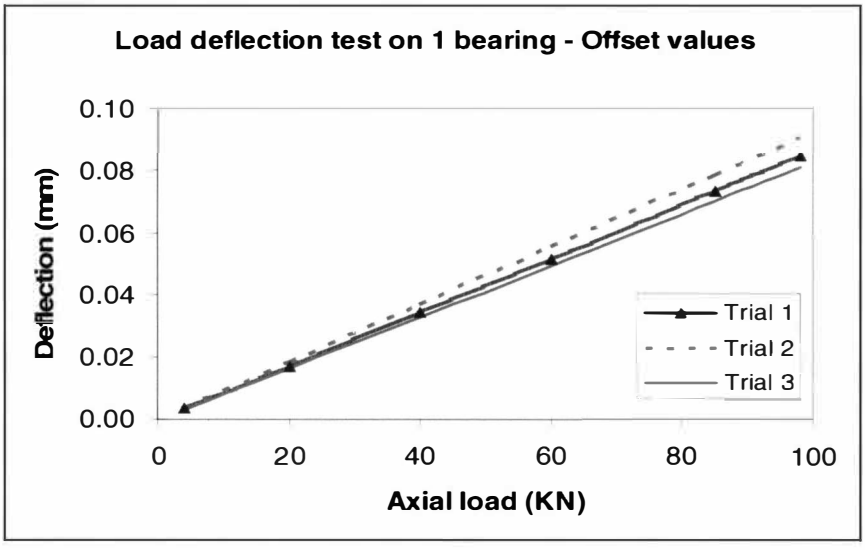

Figure 6.4: Load – deflection curve with the offset curves

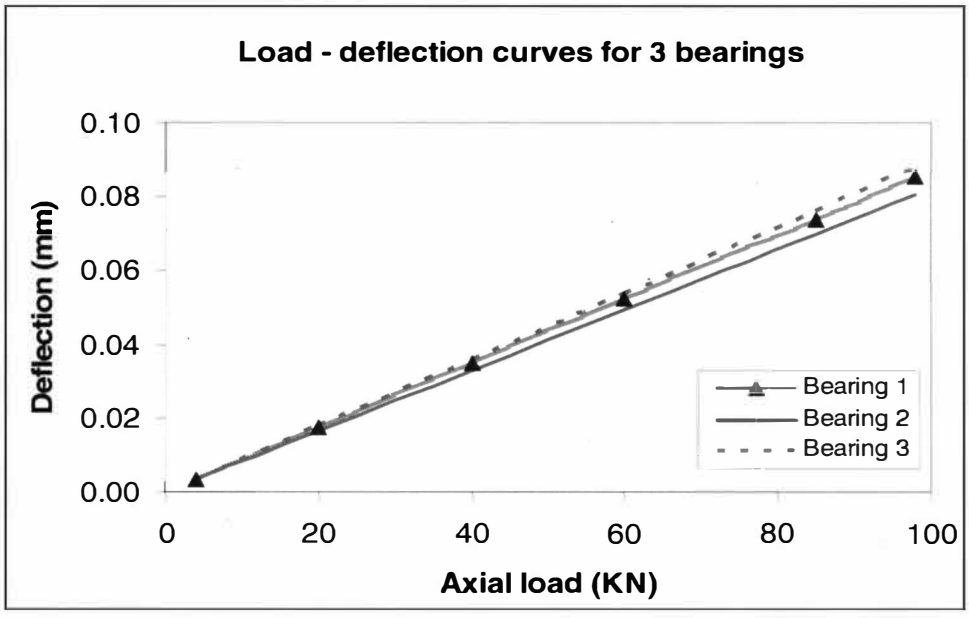

Figure 6.5: Load – deflection curve for 3 bearings of the same type

Radial load-deflection test

The specific bearing used for the analysis has been detailed below

Series : 55000

Cone : 55200C

Cup : 55437

The radial load deflection test has been done by applying an axial pre load of 15 KN and applying the radial load through the Material Testing System (MTS) machine. The axial load of 15 KN was applied by tightening the nut on the shaft. The strain gage on the shaft measured the strain across the shaft. The strain gage was connected to the strain indicator which gave the strain value directly. The displacement sensor was fitted to the housing. A probe was made to touch the surface of the shaft. When

load was applied axially, the shaft deflects, causing the movement in the probe. The sensor threaded to the housing sensed the movement of the probe and displayed the value. This displacement is the combined deflection of both the bearings.

The axial force was calculated using the expression

$$Young's \quad Modulus(E) = \frac{Stress}{Strain} \text{ , and}$$

$$Stress = \frac{Force}{Area}$$

Since the diameter of the shaft and the Young's modulus of mild steel are known, the axial force applied can be calculated.

Radial load	**Deflection**	**Axial Force**
KN	**mm**	**N**
0	0	15031.45
10	0.0015	49389.06
20	0.0025	85035.08
30	0.0035	118963.22
40	0.0045	152891.36
50	0.0055	186390.03
60	0.0065	218600.29
70	0.0075	250810.54
80	0.0085	282591.33
90	0.009	314372.12

Table 6.2: Radial load – deflection data performed for 2 bearings

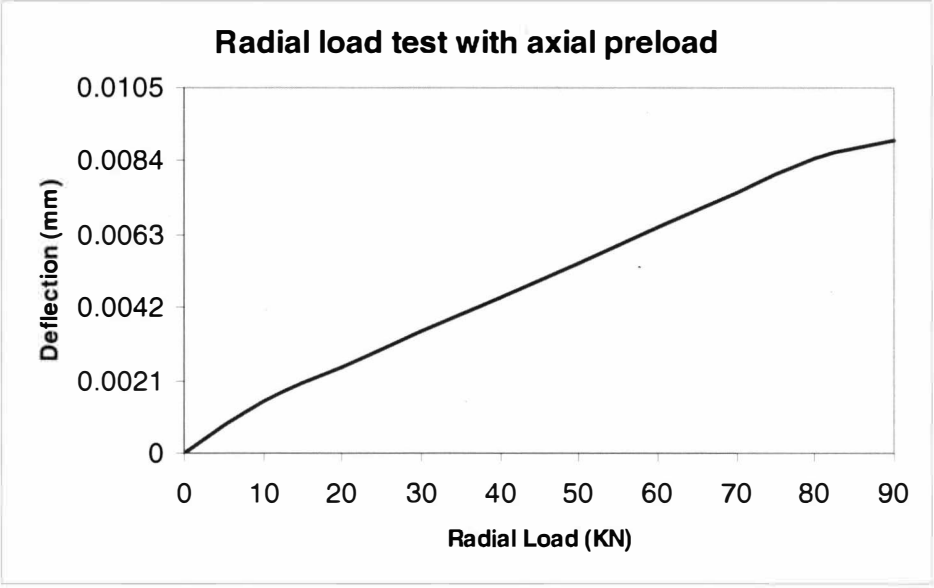

Figure 6.6: Radial load conditions with axial preload (2 bearings)

The validity of the proposed experimental method has been verified by comparing it with the values obtained from REBM software, OEM data and ABAQUS finite element model. Figure 6.6 shows the radial load – deflection slope with an axial preload of 15KN.

The variation of radial stiffness of 1 bearing was calculated from the measured stiffness of a pair of bearings. It has been plotted in Figure 6.7. The repeatability of the test system can be seen from Figure 6.8 which shows the deflection curve on 2 sets of bearings.

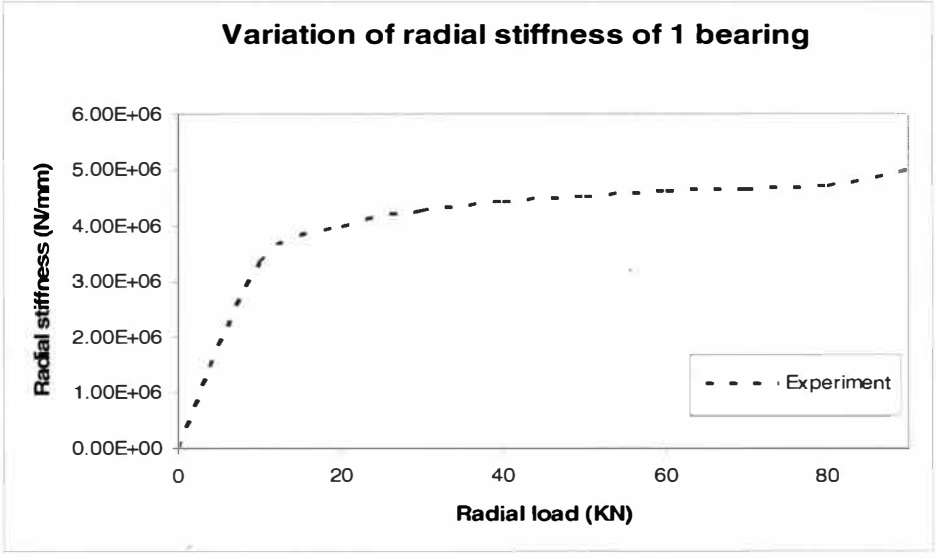

Figure 6.7: Variation of radial stiffness for 1 bearing

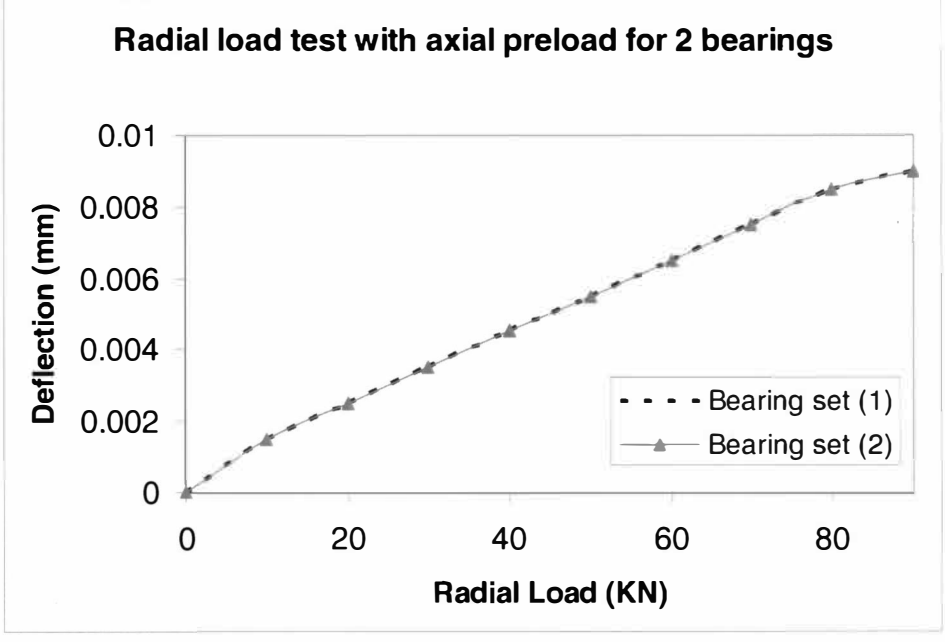

Figure 6.8: Combined radial and axial loading on 2 sets of bearings

CHAPTER VII

DISCUSSION AND COMPARISON OF RESULTS

Axial stiffness

Figure 7.1 shows the variation of axial stiffness between the four different approaches. It can be seen that the axial stiffness shown by the REBM is very much higher than the experimental approach.

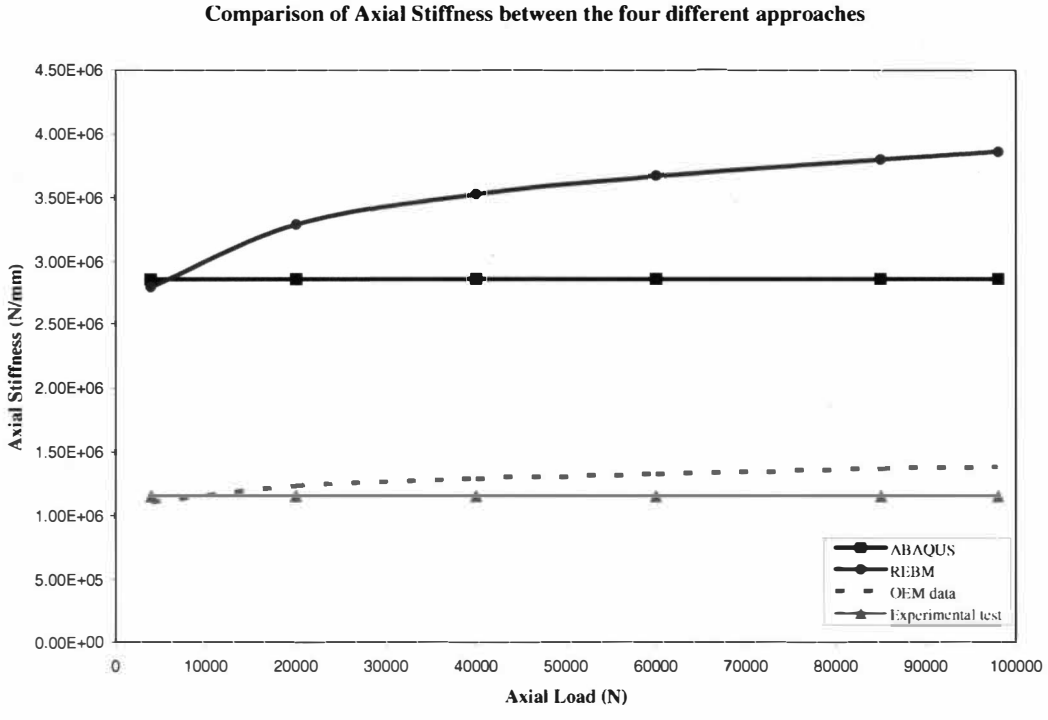

Figure 7.1: Axial stiffness variation using for different approaches

Axial Load applied	OEM Stiffness	REBM Stiffness	Measured Stiffness	% diff between REBM and test	% difference between OEM data and test
KN	N/mm	N/mm	N/mm		
4	1.11E+06	2.80E+06	1.16E+06	141.71%	4.22%
20	1.24E+06	3.29E+06	1.16E+06	184.01%	6.67%
40	1.29E+06	3.53E+06	1.16E+06	204.72%	11.47%
60	1.33E+06	3.67E+06	1.16E+06	216.81%	14.71%
85	1.37E+06	3.80E+06	1.16E+06	228.03%	18.27%
98	1.38E+06	3.86E+06	1.16E+06	233.21%	19.25%

Table 7.1: Percentage difference between the OEM data, REBM and test results

Table 7.1 shows the percentage difference between the OEM data and the measured results. It can be seen that during low loads (less than 20 KN), the difference between the axial stiffness of the OEM data and the experimental test is less than 10%. The percentage difference between REBM and test results is very high because, REBM assumes the shaft and the housing to be infinitely rigid. This causes the stiffness of the bearing to be very high when using REBM program. This can be eliminated by using the housing and shaft stiffness in the global stiffness matrix computed by REBM.

Radial stiffness

Figure 7.2 shows the variation of radial stiffness between REBM and measured test results. The radial stiffness curve follows the same trend in both the cases. But it can be seen that the percentage difference between the two cases is high during low loads (less than 20 KN) and gradually reduces at high loads. This non-linearity at loads

below 20KN is due to the fact that the shaft has been machined slightly smaller than the cone of the bearing to facilitate easy removal and also to test other bearings.

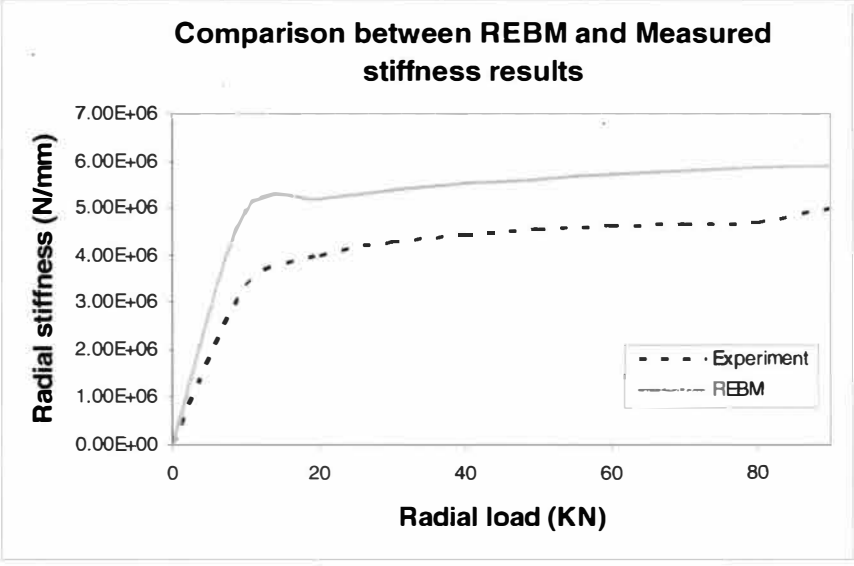

Figure 7.2: Variation of radial stiffness shown between REBM and measured test results

Radial Load applied	REBM	Measured	% difference between REBM and test
	Stiffness (Kyy)	Stiffness (Kyy)	
KN	N/mm	N/mm	
0	0.00E+00	0.00E+00	0.00%
10	4.93E+06	3.33E+06	47.82%
20	5.20E+06	4.00E+06	30.00%
30	5.38E+06	4.29E+06	25.60%
40	5.52E+06	4.44E+06	24.09%
50	5.62E+06	4.55E+06	23.69%
60	5.71E+06	4.62E+06	23.82%
70	5.79E+06	4.67E+06	24.01%
80	5.86E+06	4.71E+06	24.44%
90	5.92E+06	5.00E+06	18.37%

Table 7.2: Percentage difference between REBM and experimental test results

The percentage difference between REBM results and test results can be attributed to the fact that REBM assumes an infinitely rigid shaft and housing.

CHAPTER VIII

CONCLUSIONS AND FUTURE RESEARCH

Conclusions

Two experimental setups independent of each other were designed and manufactured to measure the translational stiffness coefficients of tapered roller bearings. The conclusions made from these studies are:

1.) The measured stiffness of the tapered roller bearings is lower than the existing mathematical and finite element models. This is due to the fact that the measured data includes the flexibility of the shaft and the housing whereas both the mathematical model and the FEA model assume the shaft and the housing to be infinitely rigid.

2.) Certain degree of non-linearity exists at loads below 20 KN, which can be due to the design of the test fixtures.

3.) The test system is repeatable.

4.) The REBM software is comparable to the combined loading (axial and radial load) performed by the experimental test system.

Future research

1.) A finite element model of any bearing can be created using the parametric Pro/E model. This allows quick generation of bearing geometry for analysis.

2.) The radial test fixture can also be used for performing vibration analysis on the shaft – bearing system. This would be useful to evaluate the rotational and rotation – translation coupling terms of the stiffness matrix.

3.) Since REBM assumes the shaft and the housing to be infinitely rigid, analysis can be done by including the shaft stiffness to the global stiffness matrix generated by REBM.

REFERENCES

1. "Modeling of Tapered Roller Bearings in Structural Analyses" DONNA J. DEMERLING, BRENT J. DORMAN, and ROBERT E. SOUTHAM, SAE Paper 84-0773.

2. T.L.H WALFORD and B.J. STONE 1980 *Journal of Mechanical Engineering Science* **22**(4), 175-181. The measurement of the radial stiffness of rolling element bearings under oscillation conditions.

3. J. S. LIN 1989 *M.S. Thesis, The Ohio State University*. Experimental analysis of dynamic force transmissibility through bearings.

4. J. KRAUS, J. J. BLECH and S.G. BRAUN 1987 *Journal of Vibration, Acoustics, Stress, and Reliability in Design, Transactions of the American Society of Mechanical Engineers* **109**, 235-240. In situ determination of rolling bearing stiffness and damping by modal analysis.

5. Y. T. SU and S. J. LIN 1993 *Journal of Sound and Vibration* **165**, 455-466. The effect of surface irregularities on roller bearing vibrations.

6. H. OHTA and N. SUGIMOTO 1996 *Journal of Sound and Vibration* **190**(2), 137-147. Vibration characteristics of tapered roller bearings.

7. M. D. RAJAB 1982 *Ph.D. Dissertation, The Ohio State University*. Modeling of the transmissibility through rolling element bearing under radial and moment loads.

8. T.C. LIM and R. SINGH 1990 *Journal of Sound and Vibration* **139**(2), 179-199. Vibration transmission through rolling element bearings. part I: bearing stiffness formulation

9. T.C. LIM and R. SINGH 1990 *Journal of Sound and Vibration* **139**(2), 201-225. Vibration transmission through rolling element bearings, part II: system studies.

10. E. P. GARGIULO 1980 *Machine Design* **52**, 107-110. A simple way to estimate bearing stiffness.

APPENDIX A

REBM WORKING MANUAL – AXIAL LOAD TEST

Black color indicates general instructions for the axial load condition.

Bold letters, underlined indicate input parameters for the particular load condition – Axial load of 4000N

1. Start REBM
2. Click "File" and then "New with wizard"
3. Choose "Roller bearing – Input Displacements"
4. Give a suitable name for the file

   Axial displacement – 4000N
5. Click "Save"
6. Enter the number of rolling elements in the bearing

   20
7. Enter the "Pitch radius" of the bearing: It is the radius measured from the centerline of the bearing to the pitch circle

   40.5
8. Enter the radial clearance between the rolling element and raceways

   0
9. Hertzian stiffness coefficient: Enter the "length of roller" and click "compute" for the software to compute the Hertzian stiffness coefficient

   Length of the roller = 18.251
10. Enter the "Unloaded contact angle", which is the cup angle

    31.128
11. Enter the "crown drop", if any

0

12. Enter the "Length of the roller"

18.251

13. Radial displacement in X direction

0

14. Radial displacement in Y direction

0

15. Axial displacement in Z direction: Guess a value and run the program. Based on the axial load it calculates, increase or decrease the guess value for the axial displacement till you get the correct axial load in the program output.

1.6e-03

16. Angular displacement about X and Y axis are set at zero.
17. Click "Finish" and then click the "Process" tab in the main window
18. The software computes the global stiffness matrix and also the angular position of the rollers

APPENDIX B

REBM WORKING MANUAL – RADIAL LOAD TEST WITH AXIAL PRELOAD

Black color indicates general instructions for the radial load condition.

Bold letters, underlined indicate input parameters for the particular load condition – axial preload of 50KN and radial load of 10 KN.

1. Start REBM
2. Click "File" and then "New with wizard"
3. Choose "Roller bearing – Input Displacements"
4. Give a suitable name for the file

   Radial load – 50KN
5. Click "Save"
6. Enter the number of rolling elements in the bearing

   20
7. Enter the "Pitch radius" of the bearing: It is the radius measured from the centerline of the bearing to the pitch circle

   40.5
8. Enter the radial clearance between the rolling element and raceways

   0
9. Hertzian stiffness coefficient: Enter the "length of roller" and click "compute" for the software to compute the Hertzian stiffness coefficient

   Length of the roller = 18.251
10. Enter the "Unloaded contact angle", which is the cup angle

    31.128

11. Enter the "crown drop", if any

    0

12. Enter the "Length of the roller"

    18.251

13. Radial displacement in X direction

    0

14. Radial displacement in Y direction: Guess a value and run the program. Based on the radial load it calculates, increase or decrease the guess value for the radial displacement till you get the correct radial load in the program output.

    2.03e-03

15. Axial displacement in Z direction: Guess a value and run the program. Based on the axial load it calculates, increase or decrease the guess value for the axial displacement till you get the correct axial load in the program output.

    1.52e-02

16. Angular displacement about X and Y axis are set at zero.
17. Click "Finish" and then click the "Process" tab in the main window
18. The software computes the global stiffness matrix and also the angular position of the rollers

APPENDIX C

AXIAL STIFFNESS CURVE FOR A BEARING LOCATED IN DIFFERENTIAL

Bearing series number		25500
Cone part number		25590
Cup part number		25523
Number of rollers		20

Table C-1: Bearing description - Differential

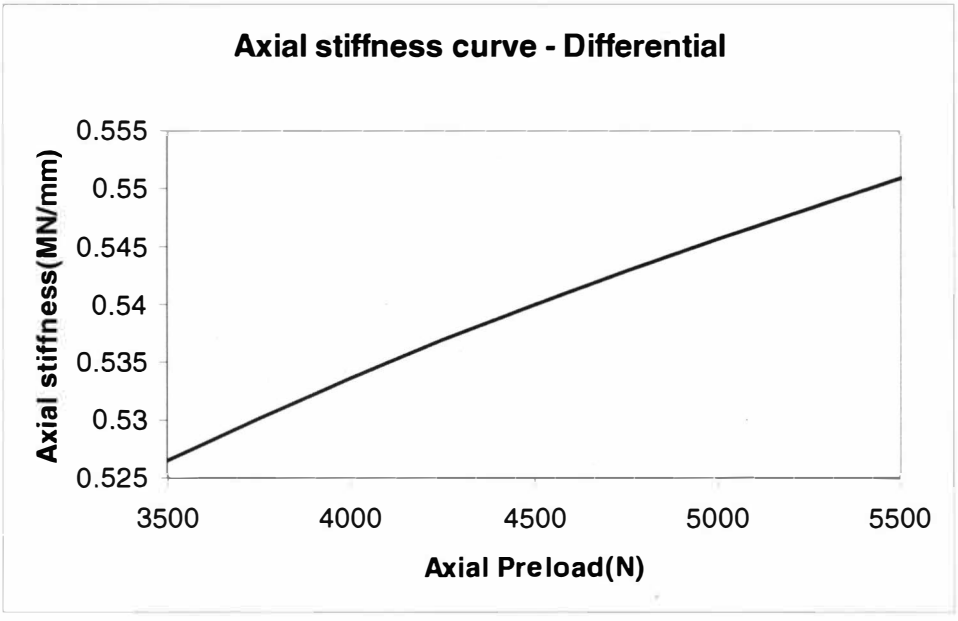

Figure C-1: Axial stiffness curve for the bearing in a differential

APPENDIX D

STIFFNESS MATRIX OF A BEARING LOCATED IN DIFFERENTIAL

DIFFERENTIAL BEARING:

Axial Preload - 3000N

(' z' is the axis of the bearing)

Mean Bearing Stiffness Matrix (X,Y,Z,RX,RY,RZ)

3.411853e+06	-5.869821e-03	5.161307e-02	-5.797511e-03	-2.634064e+07	0.000000e+00
-5.869821e-03	3.411853e+06	9.663947e-03	2.634064e+07	5.797511e-03	0.000000e+00
5.161307e-02	9.663947e-03	4.945841e+05	-1.875282e-01	-3.646511e-01	0.000000e+00
-5.797511e-03	2.634064e+07	-1.875282e-01	2.453790e+08	-9.505653e-02	0.000000e+00
-2.634064e+07	5.797511e-03	-3.646511e-01	-9.505653e-02	2.453791e+08	0.000000e+00
0.000000e+00	0.000000e+00	0.000000e+00	0.000000e+00	0.000000e+00	0.000000e+00

Axial Preload - 4000N

Mean Bearing Stiffness Matrix (X,Y,Z,RX,RY,RZ)

3.511913e+06	1.117932e-03	3.657129e-02	-1.776174e-01	-2.711315e+07	0.000000e+00
1.117932e-03	3.511913e+06	4.648996e-03	2.711314e+07	1.776174e-01	0.000000e+00
3.657129e-02	4.648996e-03	5.090889e+05	-6.614989e-03	-4.351391e-01	0.000000e+00
-1.776174e-01	2.711314e+07	-6.614989e-03	2.525753e+08	-1.262601e-01	0.000000e+00
-2.711315e+07	1.776174e-01	-4.351391e-01	-1.262601e-01	2.525753e+08	0.000000e+00
0.000000e+00	0.000000e+00	0.000000e+00	0.000000e+00	0.000000e+00	0.000000e+00

Axial Preload - 5000N

Mean Bearing Stiffness Matrix (X,Y,Z,RX,RY,RZ)

3.590640e+06	1.143705e-03	5.262085e-02	6.645027e-03	-2.772093e+07	0.000000e+00
1.143705e-03	3.590640e+06	1.415674e-02	2.772093e+07	-6.645027e-03	0.000000e+00
5.262085e-02	1.415674e-02	5.205013e+05	-1.175692e-01	-3.982057e-01	0.000000e+00
6.645027e-03	2.772093e+07	-1.175692e-01	2.582373e+08	9.668112e-01	0.000000e+00
-2.772093e+07	-6.645027e-03	-3.982057e-01	9.668112e-01	2.582373e+08	0.000000e+00
0.000000e+00	0.000000e+00	0.000000e+00	0.000000e+00	0.000000e+00	0.000000e+00

Axial Preload - 6000N

Mean Bearing Stiffness Matrix (X,Y,Z,RX,RY,RZ)

3.656942e+06	1.020752e-02	4.709803e-02	-4.572757e-02	-2.823282e+07	0.000000e+00
1.020752e-02	3.656942e+06	5.997993e-04	2.823281e+07	4.572757e-02	0.000000e+00
4.709803e-02	5.997993e-04	5.301124e+05	-1.148648e-01	-3.153496e-01	0.000000e+00
-4.572757e-02	2.823281e+07	-1.148648e-01	2.630057e+08	4.081883e-01	0.000000e+00
-2.823282e+07	4.572757e-02	-3.153496e-01	4.081883e-01	2.630057e+08	0.000000e+00
0.000000e+00	0.000000e+00	0.000000e+00	0.000000e+00	0.000000e+00	0.000000e+00

APPENDIX E

AXIAL STIFFNESS CURVE FOR A BEARING LOCATED IN PINION HEAD

Bearing series number		M802000
Cone part number		M802048
Cup part number		M802011
Number of rollers		18

Table E-1: Bearing description – Pinion head

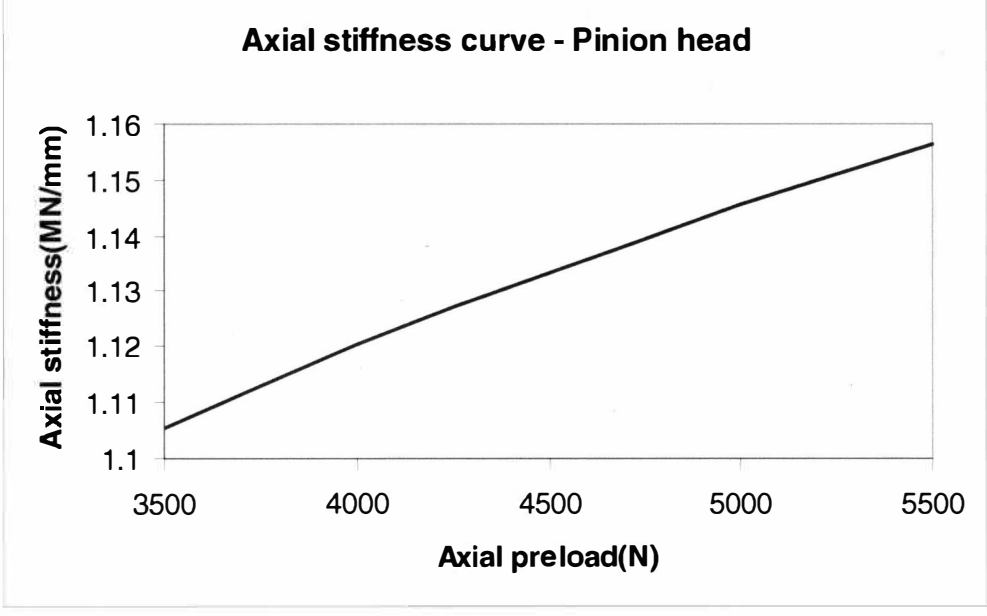

Figure E-1: Axial stiffness curve for the bearing in pinion head

APPENDIX F

STIFFNESS MATRIX OF A BEARING LOCATED IN PINION HEAD

Pinion head - 5500N

Mean Bearing Stiffness Matrix (X,Y,Z,RX,RY,RZ) ('z' is the axis of the bearing)

3.218757e+06	1.843098e-03	7.804637e-02	8.500411e-02	-3.660198e+07	0.000000e+00
1.843098e-03	3.218757e+06	7.906355e-03	3.660198e+07	-8.500411e-02	0.000000e+00
7.804637e-02	7.906355e-03	1.159904e+06	-1.228532e-01	-8.271696e-01	0.000000e+00
8.500411e-02	3.660198e+07	-1.228532e-01	4.937974e+08	-6.055943e-01	0.000000e+00
-3.660198e+07	-8.500411e-02	-8.271696e-01	-6.055943e-01	4.937974e+08	0.000000e+00
0.000000e+00	0.000000e+00	0.000000e+00	0.000000e+00	0.000000e+00	0.000000e+00

Pinion head - 5750N

Mean Bearing Stiffness Matrix (X,Y,Z,RX,RY,RZ) ('z' is the axis of the bearing)

3.233086e+06	9.495061e-03	7.486711e-02	6.446807e-02	-3.676493e+07	0.000000e+00
9.495061e-03	3.233086e+06	7.338094e-03	3.676493e+07	-6.446807e-02	0.000000e+00
7.486711e-02	7.338094e-03	1.165068e+06	-6.940725e-02	-7.286575e-01	0.000000e+00
6.446807e-02	3.676493e+07	-6.940725e-02	4.959956e+08	-2.253711e-01	0.000000e+00
-3.676493e+07	-6.446807e-02	-7.286575e-01	-2.253711e-01	4.959957e+08	0.000000e+00
0.000000e+00	0.000000e+00	0.000000e+00	0.000000e+00	0.000000e+00	0.000000e+00

Pinion head - 6000N

Mean Bearing Stiffness Matrix (X,Y,Z,RX,RY,RZ) ('z' is the axis of the bearing)

3.246872e+06	-5.154582e-03	7.989846e-02	-3.753125e-02	-3.692172e+07	0.000000e+00
-5.154582e-03	3.246872e+06	-2.335898e-03	3.692172e+07	3.753125e-02	0.000000e+00
7.989846e-02	-2.335898e-03	1.170036e+06	-1.165963e-01	-9.178297e-01	0.000000e+00
-3.753125e-02	3.692172e+07	-1.165963e-01	4.981107e+08	-1.077280e+00	0.000000e+00
-3.692172e+07	3.753125e-02	-9.178297e-01	-1.077280e+00	4.981108e+08	0.000000e+00
0.000000e+00	0.000000e+00	0.000000e+00	0.000000e+00	0.000000e+00	0.000000e+00

Pinion head - 6250N

Mean Bearing Stiffness Matrix (X,Y,Z,RX,RY,RZ) ('z' is the axis of the bearing)

3.260141e+06	1.370633e-02	6.390116e-02	1.352002e-01	-3.707258e+07	0.000000e+00
1.370633e-02	3.260139e+06	-2.669876e-03	3.707257e+07	-1.352002e-01	0.000000e+00
6.390116e-02	-2.669876e-03	1.174817e+06	-5.536843e-02	-9.313826e-01	0.000000e+00
1.352002e-01	3.707257e+07	-5.536843e-02	5.001461e+08	-1.368632e+00	0.000000e+00
-3.707258e+07	-1.352002e-01	-9.313826e-01	-1.368632e+00	5.001461e+08	0.000000e+00
0.000000e+00	0.000000e+00	0.000000e+00	0.000000e+00	0.000000e+00	0.000000e+00

Pinion head - 6500N

Mean Bearing Stiffness Matrix (X,Y,Z,RX,RY,RZ) ('z' is the axis of the bearing)

3.272959e+06	-3.544446e-03	8.038007e-02	2.595063e-02	-3.721835e+07	0.000000e+00
-3.544446e-03	3.272959e+06	9.069095e-03	3.721835e+07	-2.595063e-02	0.000000e+00
8.038007e-02	9.069095e-03	1.179436e+06	4.800996e-02	-8.075437e-01	0.000000e+00
2.595063e-02	3.721835e+07	4.800996e-02	5.021126e+08	-2.740866e+00	0.000000e+00
-3.721835e+07	-2.595063e-02	-8.075437e-01	-2.740866e+00	5.021126e+08	0.000000e+00
0.000000e+00	0.000000e+00	0.000000e+00	0.000000e+00	0.000000e+00	0.000000e+00

APPENDIX G

AXIAL STIFFNESS CURVE FOR A BEARING LOCATED IN PINION TAIL

Bearing series number		M88000
Cone part number		M88048
Cup part number		M88010
Number of rollers		16

Table G-1: Bearing description – Pinion tail

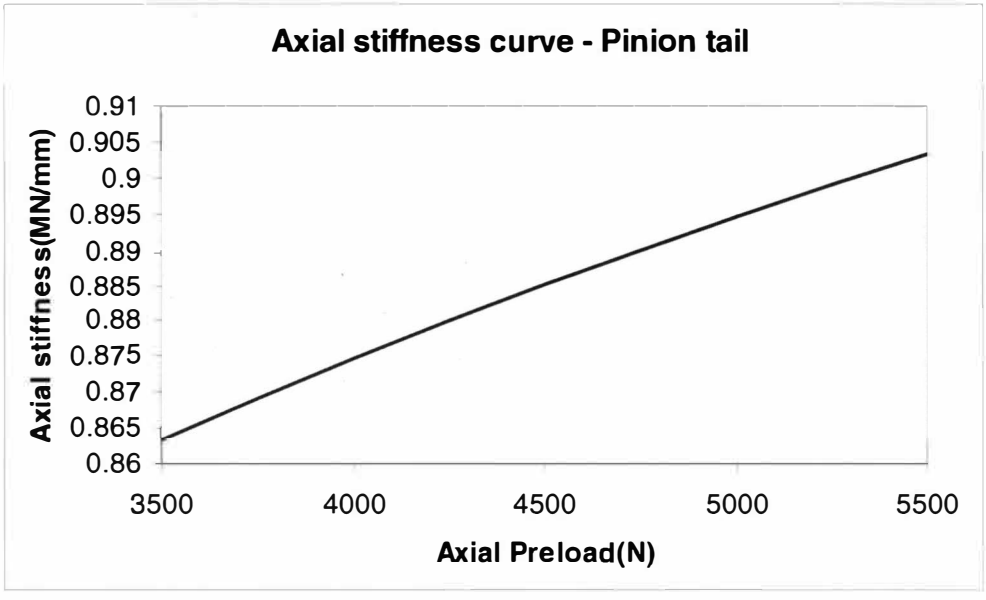

Figure G-1: Axial stiffness curve for the bearing located in pinion tail

APPENDIX H

STIFFNESS MATRIX OF A BEARING LOCATED IN PINION TAIL

Pinion tail - 5500N

Mean Bearing Stiffness Matrix (X,Y,Z,RX,RY,RZ) ('z' is the axis of the bearing)

3.457269e+06	4.968998e-03	9.055170e-02	2.367615e-01	-3.772813e+07	0.000000e+00
4.968998e-03	3.457269e+06	1.912344e-02	3.772813e+07	-2.367615e-01	0.000000e+00
9.055170e-02	1.912344e-02	1.276322e+06	1.990477e-01	-9.311997e-01	0.000000e+00
2.367615e-01	3.772813e+07	1.990477e-01	4.992378e+08	-1.384432e+00	0.000000e+00
-3.772813e+07	-2.367615e-01	-9.311997e-01	-1.384432e+00	4.992378e+08	0.000000e+00
0.000000e+00	0.000000e+00	0.000000e+00	0.000000e+00	0.000000e+00	0.000000e+00

Pinion tail - 5750N

Mean Bearing Stiffness Matrix (X,Y,Z,RX,RY,RZ) ('z' is the axis of the bearing)

3.472715e+06	4.474185e-03	8.476444e-02	1.995068e-01	-3.789670e+07	0.000000e+00
4.474185e-03	3.472715e+06	3.955639e-02	3.789670e+07	-1.995068e-01	0.000000e+00
8.476444e-02	3.955639e-02	1.282024e+06	2.770023e-01	-8.809227e-01	0.000000e+00
1.995068e-01	3.789670e+07	2.770023e-01	5.014681e+08	-1.834289e+00	0.000000e+00
-3.789670e+07	-1.995068e-01	-8.809227e-01	-1.834289e+00	5.014682e+08	0.000000e+00
0.000000e+00	0.000000e+00	0.000000e+00	0.000000e+00	0.000000e+00	0.000000e+00

Pinion tail - 6000N

Mean Bearing Stiffness Matrix (X,Y,Z,RX,RY,RZ) ('z' is the axis of the bearing)

3.487481e+06	1.801500e-02	8.662587e-02	1.733029e-01	-3.805784e+07	0.000000e+00
1.801500e-02	3.487480e+06	3.079749e-02	3.805784e+07	-1.733029e-01	0.000000e+00
8.662587e-02	3.079749e-02	1.287476e+06	-2.301455e-01	-7.758284e-01	0.000000e+00
1.733029e-01	3.805784e+07	-2.301455e-01	5.036002e+08	-2.317353e+00	0.000000e+00
-3.805784e+07	-1.733029e-01	-7.758284e-01	-2.317353e+00	5.036002e+08	0.000000e+00
0.000000e+00	0.000000e+00	0.000000e+00	0.000000e+00	0.000000e+00	0.000000e+00

Pinion tail - 6250N

Mean Bearing Stiffness Matrix (X,Y,Z,RX,RY,RZ) ('z' is the axis of the bearing)

3.501777e+06	5.076915e-03	8.992696e-02	4.440839e-02	-3.821384e+07	0.000000e+00
5.076915e-03	3.501777e+06	-1.067493e-03	3.821384e+07	-4.440839e-02	0.000000e+00
8.992696e-02	-1.067493e-03	1.292754e+06	1.438972e-01	-8.942789e-01	0.000000e+00
4.440839e-02	3.821384e+07	1.438972e-01	5.056647e+08	-1.782775e+00	0.000000e+00
-3.821384e+07	-4.440839e-02	-8.942789e-01	-1.782775e+00	5.056647e+08	0.000000e+00
0.000000e+00	0.000000e+00	0.000000e+00	0.000000e+00	0.000000e+00	0.000000e+00

Pinion tail - 6500N

Mean Bearing Stiffness Matrix (X,Y,Z,RX,RY,RZ) ('z' is the axis of the bearing)

3.515523e+06	1.111999e-02	7.667978e-02	6.282896e-02	-3.836384e+07	0.000000e+00
1.111999e-02	3.515523e+06	-1.505146e-02	3.836384e+07	-6.282896e-02	0.000000e+00
7.667978e-02	-1.505146e-02	1.297828e+06	1.431819e-01	-9.980630e-01	0.000000e+00
6.282896e-02	3.836384e+07	1.431819e-01	5.076498e+08	-3.989289e+00	0.000000e+00
-3.836384e+07	-6.282896e-02	-9.980630e-01	-3.989289e+00	5.076498e+08	0.000000e+00
0.000000e+00	0.000000e+00	0.000000e+00	0.000000e+00	0.000000e+00	0.000000e+00